iScience

CellPress

Article

Linking NMDA Receptor Synaptic Retention to Synaptic Plasticity and Cognition

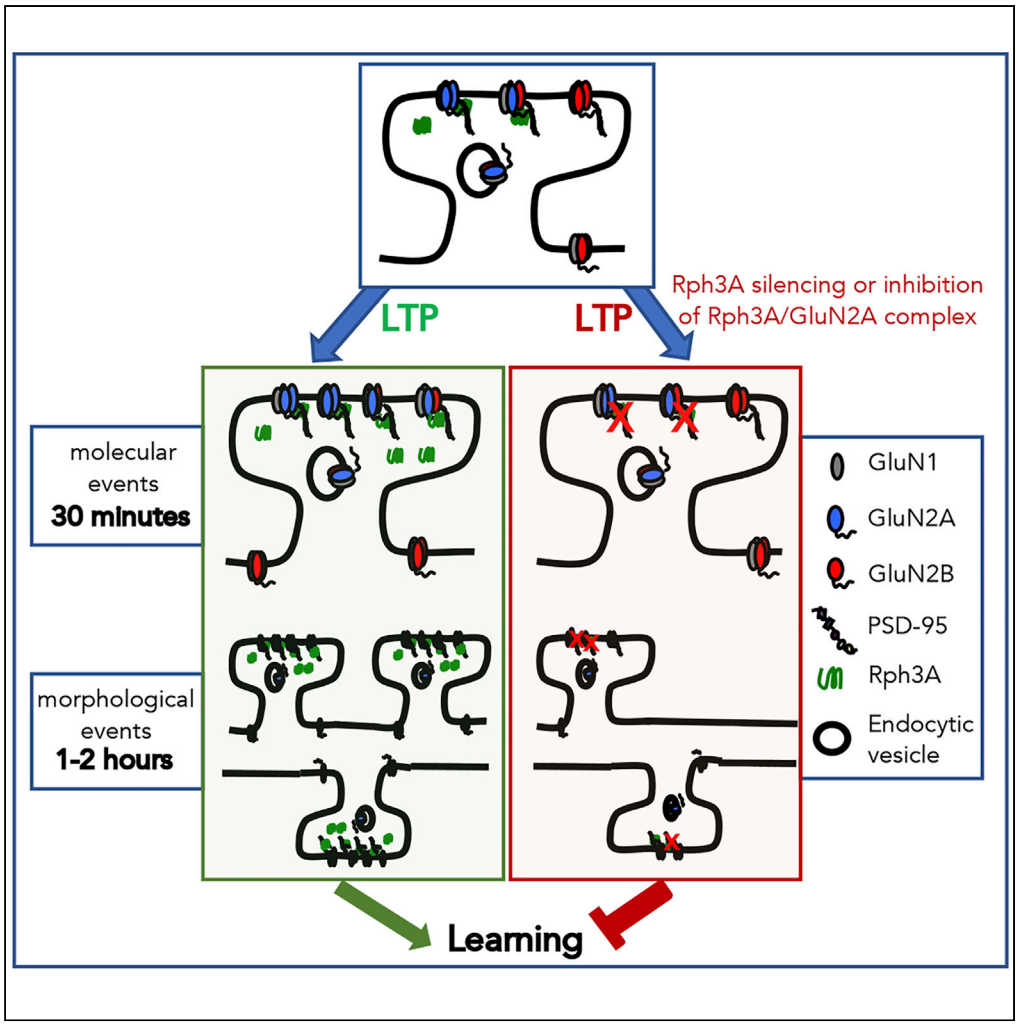

Luca Franchini, Jennifer Stanic, Luisa Ponzoni, ..., Claudia Racca, Monica Di Luca, Fabrizio Gardoni

fabrizio.gardoni@unimi.it

HIGHLIGHTS

LTP induces trafficking of Rph3A at synapses and formation of GluN2A/Rph3A complex

Disruption of Rph3A/GluN2A complex leads to LTP impairment

Rph3A/GluN2A complex is needed for modifications of dendritic spines induced by LTP

Disruption of Rph3A/GluN2A complex leads to spatial memory impairment

Franchini et al., iScience 19, 927–939
September 27, 2019
https://doi.org/10.1016/j.isci.2019.08.036

iScience

CellPress

Article

Linking NMDA Receptor Synaptic Retention to Synaptic Plasticity and Cognition

Luca Franchini,[1,7] Jennifer Stanic,[1,7,9] Luisa Ponzoni,[5,6] Manuela Mellone,[1] Nicolò Carrano,[1] Stefano Musardo,[2] Elisa Zianni,[1] Guendalina Olivero,[4] Elena Marcello,[1] Anna Pittaluga,[4] Mariaelvina Sala,[5] Camilla Bellone,[2] Claudia Racca,[3] Monica Di Luca,[1,8] and Fabrizio Gardoni[1,10,*]

SUMMARY

NMDA receptor (NMDAR) subunit composition plays a pivotal role in synaptic plasticity at excitatory synapses. Still, the mechanisms responsible for the synaptic retention of NMDARs following induction of plasticity need to be fully elucidated. Rabphilin3A (Rph3A) is involved in the stabilization of NMDARs at synapses through the formation of a complex with GluN2A and PSD-95. Here we used different protocols to induce synaptic plasticity in the presence or absence of agents modulating Rph3A function. The use of Forskolin/Rolipram/Picrotoxin cocktail to induce chemical LTP led to synaptic accumulation of Rph3A and formation of synaptic GluN2A/Rph3A complex. Notably, Rph3A silencing or use of peptides interfering with the GluN2A/Rph3A complex blocked LTP induction. Moreover, *in vivo* disruption of GluN2A/Rph3A complex led to a profound alteration of spatial memory. Overall, our results demonstrate a molecular mechanism needed for NMDAR stabilization at synapses after plasticity induction and to trigger downstream signaling events necessary for cognitive behavior.

INTRODUCTION

NMDA-type glutamate receptors (NMDARs) are key mediators of excitatory synaptic transmission in the brain (Swanger and Traynelis, 2018) contributing to synaptic plasticity and relevant for many forms of learning and memory (Morris et al., 1986; Lynch, 2004; Kullmann and Lamsa, 2007). However, the precise molecular mechanism by which postsynaptic NMDARs are retained at the synapse to allow for activity-dependent plasticity and expression of cognitive functions is still mostly unexplored.

The functional and pharmacological properties, the interacting proteins, and the subcellular localization of NMDARs strictly depend on their subunit composition, namely, the combination of the obligatory subunit GluN1 with the regulatory subunits GluN2 (A–D) and GluN3 (Paoletti et al., 2013). NMDAR subunit composition not only changes during neuronal development (Bellone and Nicoll, 2007) but at mature synapses can be modulated by synaptic activity and sensory experiences (Philpot et al., 2001, 2003; 2007; Sawtell et al., 2003; Yashiro et al., 2005) and can profoundly modify neuronal circuits and behavior. Recently, the unbalance in NMDAR subunit composition was recognized as a pivotal feature of several common neurological disorders (Sanz-Clemente et al., 2013; Lai et al., 2014; Shohami and Biegon, 2014; Gardoni and Bellone, 2015; Mellone et al., 2015).

GluN2A-containing NMDARs are rather stable at synapses, and several mechanisms have been called upon to regulate their synaptic retention. The C-terminal domain (CTD) of GluN2A enables interaction with the PDZ domain of scaffolding proteins, anchoring the receptor at the postsynaptic membrane as well as expressing correct downstream events (Horak et al., 2014; Shipton and Paulsen, 2013; Lussier et al., 2015; Stanic et al., 2015). Interestingly, mice lacking the CTD of GluN2A display impaired hippocampal long term potentiation (LTP) (Sprengel et al., 1998). Our group has previously reported Rabphilin3A (Rph3A) as a novel GluN2A synaptic partner needed to stabilize GluN2A/PSD-95 complex at the postsynaptic density (PSD). Disruption of the Rph3A/GluN2A/PSD-95 complex reduced GluN2A synaptic retention associated with increased GluN2A-containing NMDARs endocytosis (Stanic et al., 2015). Notably, this event is also associated with reduced dendritic spine density both *in vitro* and *in vivo* (Stanic et al., 2015).

[1]DiSFeB, Dipartimento di Scienze Farmacologiche e Biomolecolari, Università degli Studi di Milano, via Balzaretti 9, 20133 Milano, Italy

[2]Department of Basic Neurosciences, University of Geneva, 1211 Geneva, Switzerland

[3]Institute of Neuroscience, Newcastle University, Newcastle upon Tyne NE2 4HH, UK

[4]Department of Pharmacy, DiFAR, University of Genova, 16148 Genoa, Italy

[5]CNR Institute of Neuroscience, 20129 Milano, Italy

[6]Fondazione Zardi Gori, 20122 Milano, Italy

[7]These authors contributed equally

[8]Senior author

[9]Present address: INSERM, Neurocentre Magendie, Planar Polarity and Plasticity, U1215 Bordeaux, France

[10]Lead Contact

*Correspondence: fabrizio.gardoni@unimi.it

https://doi.org/10.1016/j.isci.2019.08.036

Many studies assigned specific roles for synaptic GluN2A-containing NMDARs in the induction of LTP and Long-Term Depression (LTD) (Liu et al., 2004; Foster et al., 2010; Kellermayer et al., 2018). Deletion of GluN2A leads to reduced hippocampal LTP and impaired spatial learning (Sakimura et al., 1995; Kiyama et al., 1998; Kannangara et al., 2015). The use of GluN2A-specific antagonists prevented LTP but not LTD (Liu et al., 2004). Similarly, selective inhibition of GluN2A-containing receptors with low Zn^{2+} concentrations impaired LTP but not LTD (Papouin et al., 2012). Finally, different studies demonstrated an increase in GluN2A-containing NMDARs at the PSD following LTP induction (Barria and Malinow, 2002; Bellone and Nicoll, 2007; Peng et al., 2010; Baez et al., 2013), suggesting that NMDAR trafficking at synapses could play a relevant role in these events. However, many open questions remain about (1) the role of the complex of proteins responsible for synaptic retention of GluN2A-containing NMDARs in synaptic plasticity and (2) the link between GluN2A-containing NMDARs and cognitive behavior. Starting from these questions here we analyzed the role of Rph3A and Rph3A/GluN2A complex in the functional and morphological modifications of excitatory synapses following induction of LTP as well as in hippocampal NMDAR-dependent behaviors such as spatial learning.

RESULTS

Rph3A-Positive Dendritic Spines Are Characterized by an Increased Spine Head Area and PSD Size

Rph3A is a known vesicle-associated presynaptic protein (Li et al., 1994; Burns et al., 1998) also highly enriched in dendritic spines at the lateral domain of the PSD (Stanic et al., 2015). Pre-embedding immunohistochemistry for Rph3A in rat *stratum radiatum* of the CA1 region of hippocampus revealed that 42.428 $\pm$ 2.301% of presynaptic terminals (n = 3632) and 48.275 $\pm$ 2.331% of dendritic spines (n = 3632) display Rph3A labeling (Figures 1A and 1B), thus indicating a similar enrichment of the protein at pre- and postsynaptic sites. We analyzed possible morphological differences between Rph3A positive (Rph3A+) and negative (Rph3A−) dendritic spines. Rph3A+ spines exhibit a highly significant increased spine head area (***$p < 0.001$; Figures 1C and 1D and Table 1) and PSD length (***$p < 0.001$; Figures 1E and 1F and Table 1) and also an augmented PSD thickness (*$p < 0.05$; Figures 1G and 1H and Table 1) compared to Rph3A− ones, thus defining a selective accumulation of the protein in more "mature" synapses.

Modulation of Rph3A/GluN2A Complex by Long-Term Potentiation

It is well known that induction of LTP leads to an accumulation of GluN2A-containing NMDARs at the excitatory PSDs (Barria and Malinow, 2002; Grosshans et al., 2002; Bellone and Nicoll, 2007). By using a previously validated protocol, here we treated rat primary hippocampal neurons with Forskolin/Rolipram/Picrotoxin cocktail to induce chemical LTP (cLTP; Otmakhov et al., 2004; Dinamarca et al., 2016). Quantification of GluA1 Ser845 phosphorylation showed a significant increase of AMPA subunit phosphorylation levels after cLTP (Esteban et al., 2003; Oh et al., 2006; Hu et al., 2007; Makino et al., 2011; Figure S1). We observed that cLTP was sufficient to increase the levels not only of GluN2A (**$p < 0.01$; Figure 2A) but also of Rph3A (*$p < 0.05$; Figure 2A) in postsynaptic membrane fractions (Triton insoluble fractions, TIF; Gardoni et al., 2006) as measured 15 min after cLTP induction. Conversely, induction of cLTD (Oh et al., 2006; Marcello et al., 2013) did not induce any modification of GluN2A and Rph3A synaptic localization (Figure S2).

The confocal microscopy analysis in GFP-transfected primary hippocampal neurons revealed that cLTP significantly increased the percentage of Rph3A+ spines compared with basal conditions (Figure 2B; **$p < 0.01$). A careful morphological analysis of dendritic spines showed that Rph3A was selectively enhanced in mushroom spines after cLTP (Figure 2C; *$p < 0.05$); no alteration of Rph3A localization was observed in stubby or thin spines (Figure 2C).

We performed Proximity Ligation Assay (PLA) to address whether Rph3A accumulation in spines leads also to its interaction with the GluN2A/PSD-95 complex (Stanic et al., 2015). Analysis of PLA clusters after cLTP in GFP-transfected neurons (Figure 2D) showed a statistically significant increase in Rph3A/PSD-95 (**$p < 0.01$) and GluN2A/Rph3A (*$p < 0.05$) interactions within dendritic spines.

The observed increase of Rph3A levels at postsynaptic sites after cLTP induction could be the result of a modulation of protein trafficking or novel protein synthesis. To clarify this point, we blocked protein synthesis through anisomycin (40 μM) during cLTP. Protein levels of GluN2A and Rph3A at synapses did not differ in the presence or absence of anisomycin (Figure 2E), thus suggesting that novel protein synthesis does not play a key role in these events. To confirm these results, we performed analysis of Rph3A local synthesis after cLTP through a PLA of puromycin and Rph3A (puro-PLA assay; see Transparent Methods).

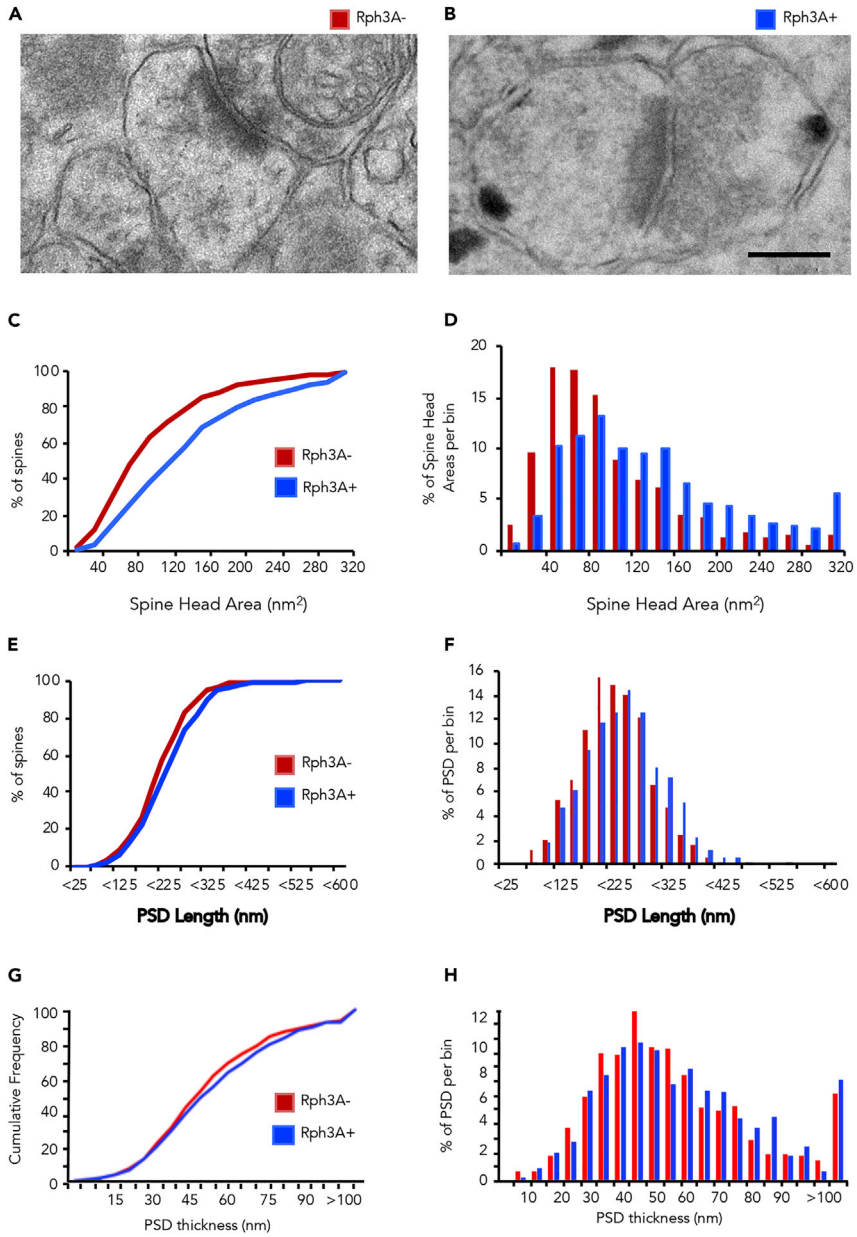

Figure 1. Morphological Analysis of Rph3A-Positive and Rph3A-Negative Dendritic Spines

(A and B) Representative electron micrographs of *stratum radiatum* CA1 region of Rph3A negative (A, left image; Rph3A−) and positive (B, right image; Rph3A+) spinous synapses, respectively. Scale bar, 125 nm.

(C and D) Shifted distribution of spine head area toward bigger values in Rph3A+ spines (blue; n = 689/1,500, 3 rats) compared with Rph3A− spines (red; n = 811/1,500, 3 rats; $p < 0.001$, Mann-Whitney Rank Sum Test).

(E and F) Shifted distribution of PSD length toward bigger values in Rph3A+ spines (blue; n = 689/1,500, 3 rats) compared with Rph3A− spines (red; n = 811/1,500, 3 rats; $p < 0.001$, Mann-Whitney Rank Sum Test).

(G and H) Shifted distribution of PSD thickness toward bigger values in Rph3A+ spines (blue; n = 689/1,500, 3 rats) compared with Rph3A− spines (red; n = 811/1,500, 3 rats; $p < 0.05$; Mann-Whitney Rank Sum Test).

This assay allows one to monitor the synthesis of novel Rph3A molecules in the different subcellular compartments (Dieck et al., 2015). As shown in Figure 2F, we did not observe any difference in the density of puromycin/Rph3A clusters between control and cLTP-treated neurons both in the soma and along dendrites. Overall, these *in vitro* data indicate that the cLTP-triggered accumulation of GluN2A/Rph3A/PSD-95 complexes at synapse cannot be ascribed to Rph3A *de novo* synthesis.

Labeling	Rph3A− Spines (n = 811/1,500)	Rph3A+ Spines (n = 689/1,500)	p Value (Rph3A+ versus Rph3A−)
PSD length (nm)	215 ± 2.38	232 ± 2.87	<0.001
PSD thickness (nm)	54.5 ± 0.96	56.7 ± 1.06	0.049
Spine Head Area (nm^2)	99.9 ± 2.40	143 ± 3.54	<0.001

Table 1. Morphological Analysis of Rph3a+ and Rph3A− Dendritic Spines (n = 3 Rats, 500 Spines/Rat)

Housing animals in enriched environment conditions induces neuronal plasticity events and accumulation of GluN2A-containing NMDARs at synapses (Philpot et al., 2001, 2003; 2007; Sawtell et al., 2003; Yashiro et al., 2005; Grilli et al., 2009; Summa et al., 2011; Bonfiglio et al., 2018). To evaluate whether Rph3A localizes at the postsynapse also after this *in vivo* plasticity, we purified the postsynaptic fraction from hippocampi of mice housed in enriched environment for 3 months or in standard cages. As previously reported, enriched environment promoted the increase of GluN2A-containing NMDARs at synapses (Figure 2G; *p < 0.05; Philpot et al., 2001, 2003, 2007; Sawtell et al., 2003; Yashiro et al., 2005). Similarly, the enriched environment induced also a significant increase of Rph3A levels in the postsynaptic fraction (Figure 2G; *p < 0.05).

Phospholipase C Activation Promotes Rph3A/GluN2A Interaction in the Postsynaptic Density

Different putative molecular mechanisms could be envisaged for the increased formation of the synaptic Rph3A/GluN2A complex induced by LTP. It is well known that LTP induces activation of tyrosine kinases (src/fyn) in the postsynaptic compartment leading to phosphorylation of NMDAR subunits (Nakazawa et al., 2001; Liu et al., 2004). In particular, GluN2A phosphorylation at Tyr1387, within the GluN2A domain involved in the interaction with Rph3A (Stanic et al., 2015), has been put forward for consideration (Yang and Leonard, 2001). However, as shown in Figure S3A, cLTP did not change the phosphorylation of GluN2A Tyr1387 in cultured cells. Moreover, co-localization analysis in COS-7 cells transfected with Rph3A and GluN2Awt/GluN2A-Y1387E (mimicking phosphorylation) showed that GluN2A phosphorylation in this tyrosine residue did not alter the capability of the subunit to interact with Rph3A (Figure S3B). Overall, these experiments indicate that GluN2A phosphorylation in Tyr1387 does not represent the molecular event regulating GluN2A/Rph3A complex formation following LTP induction.

Rph3A, through both its C2A and C2B domains, binds inositol triphosphate (IP3) in a Ca^{2+}-dependent manner (Montaville et al., 2008; Ferrer-Orta et al., 2017). Interestingly, IP3 and Ca^{2+} binding to the C2A domain are reciprocally modulated in a positive manner. In particular, Ca^{2+} induces a conformational rearrangement of a specific Rph3A loop (namely, CBL3), which is involved in IP3 binding (Coudevylle et al., 2008; Guillén et al., 2013). Notably, IP3 and Ca^{2+} regulate also the formation of Rph3A complex with GluN2A (Stanic et al., 2015). Phospholipase C (PLC) cleaves phosphatidylinositol 4,5-bisphosphate (PIP2) into IP3 and diacylglycerol; afterward, IP3 releases Ca^{2+} from the ER, suggesting that activation could modulate the formation of Rph3A/GluN2A. PLCγ and PLCβ isoforms are both localized at the excitatory synapse and functionally associated to TrkB (Gottschalk et al., 1999) and group I metabotropic receptors (mGluR1/mGluR5; Chuang et al., 2001; Hannan et al., 2001), respectively. Activation of group I of metabotropic glutamate receptors (mGluRs) through DHPG (50 μM) increased postsynaptic levels of both Rph3A (Figure 3A, *p < 0.05) and GluN2A (Figure 3A, *p < 0.05) but not GluN2B (Figure 3A). Under the same experimental conditions, DHPG augmented Rph3A-GluN2A interaction as evaluated by the co-immunoprecipitation assay (Figure 3B, ***p < 0.001). Analysis of pERK phosphorylation was performed as a positive control of DHPG treatment (Gallagher et al., 2004; Figure S4, **p < 0.01).

Finally, as further demonstration of the role of PLC in the modulation of Rph3A retention at the excitatory synapse, we showed that also the treatment of hippocampal primary cultures with the TrkB agonist Brain Derived Neurotrophic Factor (BDNF, 3 h, 50 ng/mL), leading to activation of the PLCγ pathway, increased Rph3A protein levels in the postsynaptic fraction (Figure 3C, *p < 0.05).

Modulation of Rph3A/GluN2A Complex Governs Plasticity at Molecular and Structural Level

To test the direct role of Rph3A in the membrane localization of GluN2A-containing NMDARs following induction of cLTP, we used a small hairpin RNA for Rph3A (tGFP-shRph3A) to downregulate Rph3A in

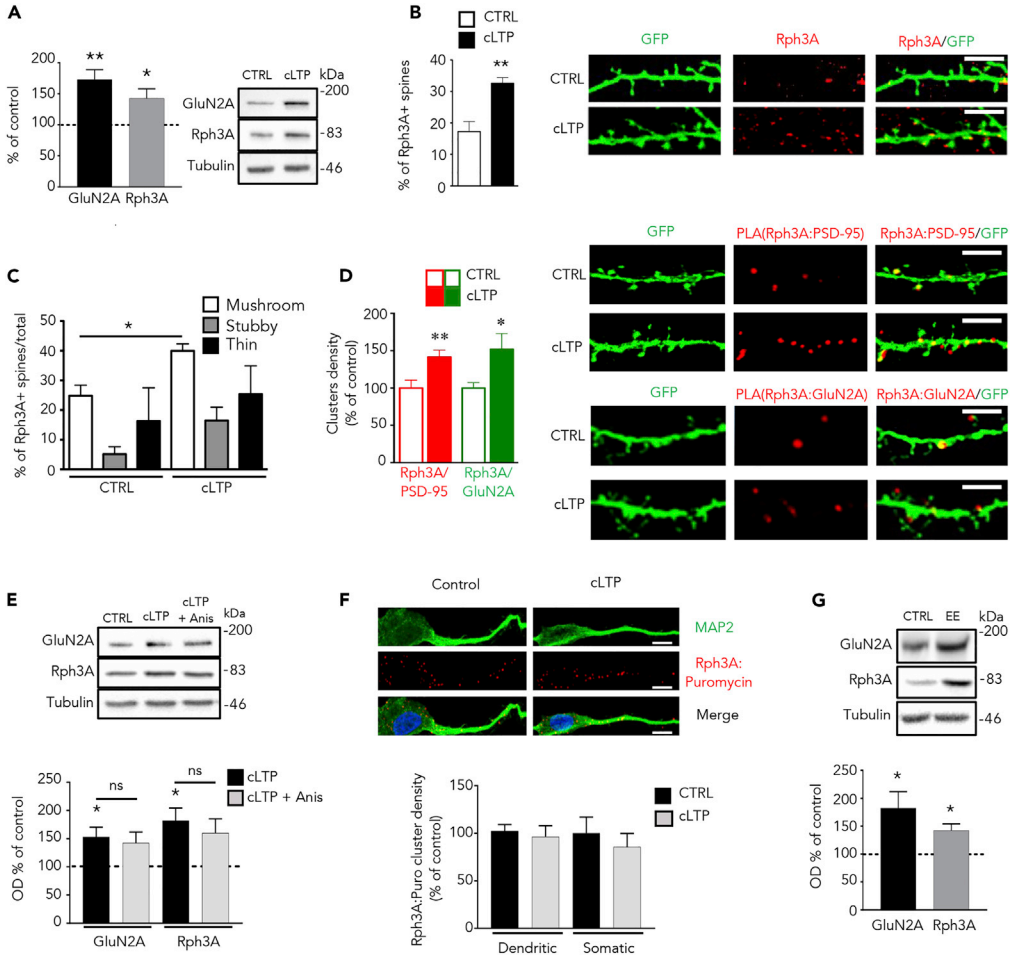

Figure 2. Effect of Long-Term Potentiation on Rph3A/GluN2A Complex

(A) Bar chart (left) and representative western blots (right) for GluN2A and Rph3A protein levels in TIF from hippocampal primary cultures after cLTP. cLTP induction was performed in artificial cerebrospinal fluid (ACSF) without $MgCl_2$, plus 50 μM Forskolin, 0.1 μM Rolipram, and 100 μM Picrotoxin for 16 min. Control groups were kept in normal ACSF. After that, cells were incubated back in ACSF with $MgCl_2$ for 15 min (n = 9, t test; *p < 0.05; **p < 0.01; data are expressed as mean ± SEM). Molecular weight markers are indicated on the right.

(B) Dendritic spine positivity for Rph3A after cLTP in primary cultures (t test) and representative images (scale bar, 5 μm). **p < 0.01; data are expressed as mean ± SEM.

(C) Morphological analysis of Rph3A-positive spines before and after cLTP treatment (t test). *p < 0.05; data are expressed as mean ± SEM.

(D) Bar chart and representative images of PLA for Rph3A:PSD-95 (red bar) and Rph3A:GluN2A (green bar) in control cultures (CTR) and after cLTP (scale bar, 5 μm). Merge panels are shown in the right. *p < 0.05; **p < 0.01; data are expressed as mean ± SEM.

(E) Bar graph and representative blots of GluN2A and Rph3A protein levels in TIF from hippocampal cultures after cLTP, with (cLTP + Anis) or without (cLTP) protein synthesis inhibitor Anisomycin (40 μM) (RM one-way ANOVA, n = 8); *p < 0.05; data are expressed as mean ± SEM. Molecular weight markers are indicated on the right.

(F) Column graph and representative images of Puro-PLA analysis for Rph3A newly synthetized (Rph3A:puromycin) in dendritic and somatic compartments after cLTP in primary cultures (n = 39–43, scale bar, 10 μm).

(G) Bar graph and representative images of GluN2A and Rph3A protein levels in hippocampal TIF from young mice housed in enriched environment (EE) compared with standard cages (CTRL). *p < 0.05; data are expressed as mean ± SEM. Molecular weight markers are indicated on the right.

the presence or absence of cLTP induction, and we evaluated the surface localization of the GluN2A subunit (Figure 4A). As expected (Baez et al., 2018), induction of cLTP promoted an accumulation of GluN2A at the cell surface (Figure 4A, ***p < 0.001). Notably, Rph3A silencing prevented GluN2A accumulation at the cell surface following induction of cLTP (Figure 4A, ***p < 0.001 shSCR-cLTP versus shRph3A-cLTP), thus

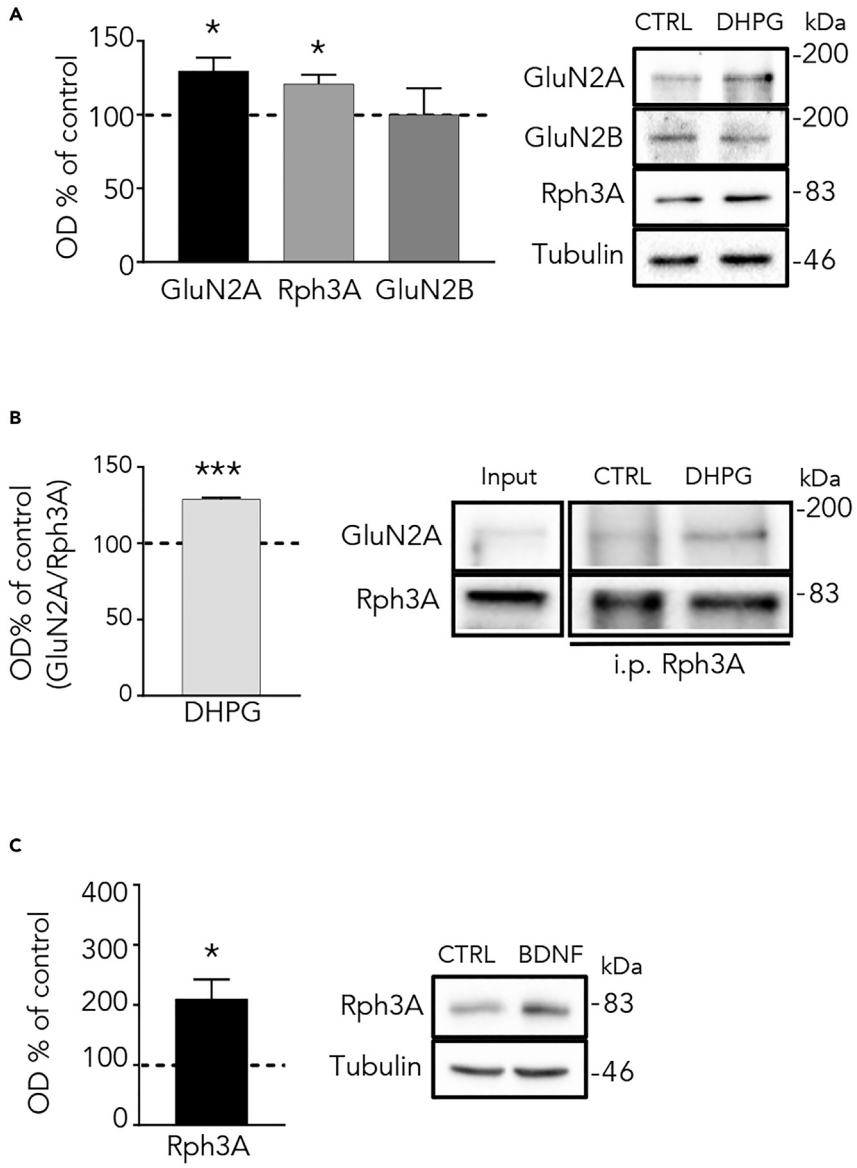

Figure 3. mGluR/PLC Pathway Modulates Rph3A Synaptic Localization and Interaction with NMDAR

(A) Column chart and representative blots in TIF from primary cultures treated with 3,5-R,S-DHPG (DHPG, 50 μM for 15 min). DHPG increased GluN2A and Rph3A significantly, whereas no difference could be inferred for GluN2B (t test, n = 5). *$p < 0.05$; data are expressed as mean ± SEM. Molecular weight markers are indicated on the right.

(B) Graph and blots for co-immunoprecipitation of Rph3A and GluN2A from P2 fraction of primary cultures treated with DHPG. The analysis revealed increased binding of Rph3A with GluN2A (n = 4). ***$p < 0.001$; data are expressed as mean ± SEM. Molecular weight markers are indicated on the right.

(C) Bar graph and representative blots for Rph3A and tubulin in TIF from primary hippocampal neurons treated with BDNF (50 ng/mL, 3 h; n = 5; t test). *$p < 0.05$; data are expressed as mean ± SEM. Molecular weight markers are indicated on the right.

suggesting that formation of GluN2A/Rph3A complex is required for the stabilization of GluN2A at synapses following LTP.

It is well known that LTP also increases GluA1 clusters at synapses (Malinverno et al., 2010). As shown in Figures 4B and 4C, induction of cLTP increased GluA1 cluster width (Figure 4B, ***$p < 0.001$), paralleled by augmented spine density (Figure 4C, **$p < 0.01$) and spine head width (Figure 4C, *$p < 0.05$).

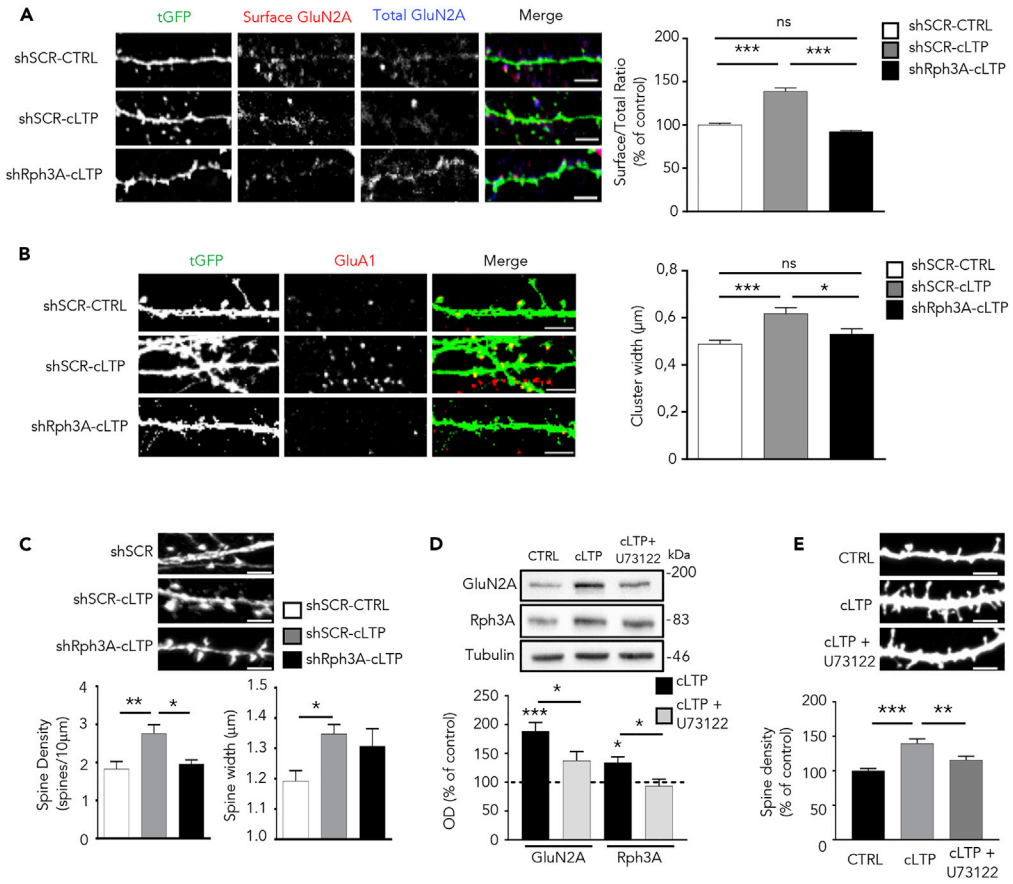

Figure 4. Effect of Modulation of Rph3A/PLC Pathway on GluN2A Surface Staining, GluA1 Synaptic Localization and Spine Morphology

(A) Bar graph and representative images of GluN2A surface expression before (CTRL) and after cLTP (cLTP) in tGFP-shScramble (shSCR) or tGFP-shRph3A transfected neurons. cLTP induction was performed in ACSF without $MgCl_2$, plus 50 µM Forskolin, 0.1 µM Rolipram and 100 µM Picrotoxin for 16 min. Control groups were kept in normal ACSF. After that, cells were incubated back in ACSF with $MgCl_2$ for 15 min (one-way ANOVA Tukey post hoc n = 41–46, scale bar, 4 µm); ***p < 0.001.

(B) Graph chart and representative images of GluA1 cluster width before and after cLTP in hippocampal neurons transfected with shSCR or shRph3A (one-way ANOVA Tukey post hoc, n = 9–11, scale bar, 4 µm); *p < 0.05, ***p < 0.001.

(C) Column graphs and representative images of shSCR or shRph3A transfected neurons before and after cLTP. cLTP induction was performed in ACSF without $MgCl_2$, plus 50 µM Forskolin, 0.1 µM Rolipram, and 100 µM Picrotoxin for 16 min. Control groups were kept in normal ACSF. After that, cells were incubated back in ACSF with $MgCl_2$ for 2 h (one-way ANOVA Tukey post hoc, n = 8, scale bar, 4 µm); **p < 0.01, *p < 0.05.

(D) Inhibition of Phospholipase C with U73122 (1 µM) during cLTP on hippocampal primary cultures recapitulates control levels of Rph3A and GluN2A in TIF (one-way ANOVA Bonferroni post hoc, n = 5–7); *p < 0.05, ***p < 0.001. Molecular weight markers are indicated on the right.

(E) Bar chart and representative images of spine morphology analysis after cLTP induction in the presence (cLTP + U73122) or absence (cLTP) of U73122 (1 h after cLTP; one-way ANOVA Bonferroni post hoc, n = 25, scale bar, 4 µm); **p < 0.01. ***p < 0.001.

Interestingly, Rph3A silencing completely prevented any modification of GluA1 cluster size (Figure 4B, *p < 0.05 shSCR-cLTP versus shRph3A-cLTP) and spine density (Figure 4C, *p < 0.05 shSCR-cLTP versus shRph3A-cLTP). Moreover, Rph3A silencing prevented the enlargement of spine head width induced by LTP (Figure 4C, p > 0.05, shSCR-CTRL versus shRph3A-cLTP).

To evaluate the role of PLC in these events, we inhibited PLC activity through U73122 (1 µM) during cLTP. Co-incubation with PLC inhibitor recapitulated basal levels of both Rph3A (*p < 0.05, U73122 + cLTP versus cLTP) and GluN2A (*p < 0.05, U73122 + cLTP versus cLTP) in the postsynaptic fraction (Figure 4D). It is well

known that LTP increases dendritic spine density in hippocampal neurons (Chidambaram et al., 2019). In addition, we previously reported that Rph3A silencing or disruption of its interaction with GluN2A is sufficient to reduce spine density in resting conditions (Stanic et al., 2015). Notably, we now observed that inhibition of PLC with U73122 during cLTP not only decreased synaptic localization of Rph3A/GluN2A complex (Figure 4D) but also completely blocked the increase in dendritic spine density produced by cLTP (Figure 4E; ***$p < 0.001$ cLTP versus control; **$p < 0.01$ cLTP versus cLTP + U73122). Overall, these results suggest that PLC activation is required to modulate Rph3A/GluN2A retention at synapses needed for structural modifications following induction of LTP in primary hippocampal neurons.

Overall, the above-described results indicate that induction of cLTP in primary hippocampal neurons promotes synaptic enrichment of the Rph3A/GluN2A complex, demonstrating also a key role for Rph3A in LTP-dependent molecular and morphological modifications of dendritic spines, namely, LTP-dependent trafficking of AMPARs and formation of novel dendritic spines.

GluN2A/Rph3A Complex Is Necessary for LTP Induction and Spatial Learning

We previously reported that perturbing GluN2A/Rph3A interaction *in vivo* with TAT-2A40 interfering peptide (containing the GluN2A1349-1389 domain involved in the interaction with Rph3A) decreases the amplitude of NMDAR-mediated currents and GluN2A levels at dendritic spines (Stanic et al., 2015, 2017). Here, we acutely treated adult mice with TAT-2A40 or its control TAT-scramble (TAT-SCR) peptide (3 nmol/g, i.p., single injection). One hour after the treatment, animals were sacrificed for *ex vivo* molecular and electrophysiological analyses. As previously reported (Stanic et al., 2015, 2017), treatment with TAT-2A40 leads to a specific reduction of GluN2A but not GluN2B subunits at synapses leading to an overall significant decrease of synaptic GluN2A/GluN2B ratio with no modification of GluN1 (see Figure S5). LTP was induced by stimulation of Schaffer collaterals in CA1 *stratum radiatum* (see Transparent Methods). As expected, in hippocampal slices from animals treated with TAT-SCR peptide we observed the induction and the maintenance of the LTP (Figures 5A–5C). On the contrary, in hippocampal slices from animals treated with TAT-2A40 peptide, LTP induction was completely impaired (Figures 5A–5C; **$p < 0.01$).

Changes in NMDAR synaptic levels are triggered by synaptic plasticity and by spatial memory formation (Baez et al., 2018). In particular, an increase in the synaptic GluN2A/GluN2B subunit ratio could act as a stabilizer of synaptic/circuital changes, hence leading to stabilization of memory consolidation, particularly spatial representations (Baez et al., 2018). Starting from these considerations, we performed a spatial object recognition behavioral task to assess the effect of disrupting Rph3A/GluN2A interaction on spatial learning, in the same experimental conditions used for electrophysiology (TAT-2A40 versus TAT-SCR, 3 nmol/g, i.p., single injection). In the Spatial Object Recognition test, locating the object to a novel configuration during the T2 phase induced a significant treatment effect in terms of mean discrimination index between TAT-SCR- and TAT-2A40-treated mice ($t18 = 5.61$, ***$p < 0.0001$, Figure 5D). During T1 phase, all groups of mice showed a similar mean exploration time for each object (TAT-SCR: Object 1 = 11.7 $\pm$ 1.0; Object 2 = 12.4 $\pm$ 0.96. TAT-2A40: Object 1 = 12.9 $\pm$ 0.82; Object 2 = 13.7 $\pm$ 0.75). During T2 phase two-way ANOVA revealed differences among groups (treatment effect: $F(1,36) = 4.269$, $p < 0.05$; object effect: $F(1,36) = 8.79$, $p = 0.0053$; interaction treatment x object: $F(1,36) = 12.28$, $p = 0.001$). Post hoc analysis revealed that the mean exploration time of the displaced object was significantly higher than that of the stationary object after treatment with TAT-SCR (Figure 5E; $^{\$\$\$}p < 0.001$ versus the corresponding stationary object). Conversely, no difference was shown in the mean exploration time between the two objects after treatment with TAT-2A40 (Figure 5E). The mean number of horizontal and vertical movements did not change between the two groups (Horizontal counts: $t18 = 1.252$, $p = 0.23$, Figure 5F; Vertical counts: $t18 = 0.325$, $p = 0.74$, Figure 5G).

DISCUSSION

The mechanism by which GluN2A-containing NMDARs accumulate at the synapse following activity-dependent plasticity and how this relates to the expression of given cognitive functions has been approached. Here we indicate that the formation of the Rph3A/GluN2A complex is needed for molecular and structural modifications of dendritic spines induced by LTP. *In vivo* disruption of Rph3A/GluN2A interaction by an interfering peptide leads to both LTP and spatial memory impairment corroborating this finding.

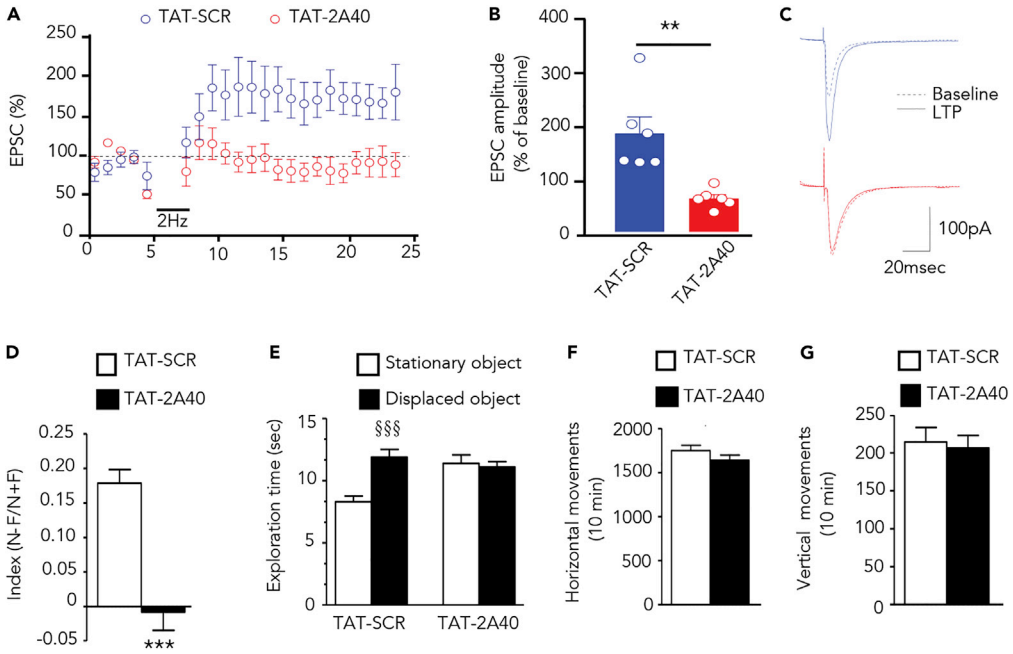

Figure 5. *In Vivo* Effect of Rph3A/GluN2A Interfering Peptide on LTP Induction and Spatial Memory

(A–C) Somatic whole-cell voltage-clamp recordings were made from CA1 pyramidal cells using 2–6 ΩM electrodes. The internal solution contained (in mM) 115 $CsMeSO_4$, 20 $CsCl_2$, 10 HEPES, 2.5 $MgCl_2$, 4 NaATP, 0.4 NaGTP, 10 NaCreatine, and 0.6 EGTA (pH 7.2). Synaptic responses were collected with a Multiclamp 700B amplifier (Axon Instruments, Foster City, CA, USA), filtered at 2 kHz, digitized at 5 kHz, and analyzed online using Igor Pro Software (Wavemetrics, Lake Oswego, OR, USA). All data are expressed as mean ± SEM. Cells were held at −70 mV, and LTP protocol was induced by pairing the cell at 0 mV at a frequency of 2 Hz for 90 s. The amplitude of TAT-2A40 treated animals, as well as LTP kinetic, was completely impaired compared with TAT-SCR (AMPLITUDE, **$p < 0.01$, unpaired t test).

(D and E) Mean discrimination index and mean exploration time evaluated in the Spatial Object Recognition test, 60 min after treatment; ***$p < 0.001$ versus TAT-SCR Student's t test; §§§$p < 0.001$ versus corresponding stationary object, TAT-SCR; two-way ANOVA followed by Bonferroni test.

(F and G) Cumulative mean of horizontal (F) and vertical (G) counts evaluated for 10 min in an automated activity cage. N = 10 animals for each group.

Rph3A is a Rab effector protein involved in neurotransmitter release at the presynaptic terminal, and its conformation and activity are strictly modulated by the presence of Ca^{2+} ions and IP3 (Coudevylle et al., 2008; Montaville et al., 2008; Guillén et al., 2013). Recently, Rph3A has been detected also at dendritic spines, where it interacts with and promotes synaptic retention of GluN2A-containing NMDARs (Stanic et al., 2015). Here we explored the molecular mechanisms by which Rph3A binds the GluN2A subunits following different paradigms of activity-dependent plasticity induced both *in vitro*, as cLTP or mGluR5 activation, and *in vivo* through enriched environment. All these forms of plasticity converge on promoting Rph3A accumulation at dendritic spines and its Ca^{2+}/IP3-dependent interaction with the NMDAR subunit.

Our electron microscopy data eventually clarify the pre- and postsynaptic enrichment of Rph3A. We show by pre-embedding immunohistochemistry that about half of presynaptic terminals as well as dendritic spines in hippocampus display Rph3A, thus suggesting a similar distribution of the protein at the two sides of the excitatory synapse. Importantly, we observed that spines in which we detect Rph3A have an increased spine head area and PSD length and thickness, suggesting a higher stability of neuronal transmission through these Rph3A-positive connections.

Accumulation of GluN2A-containing NMDARs at synapse is a highly validated molecular event occurring after LTP induction (Barria and Malinow, 2002; Grosshans et al., 2002; Bellone and Nicoll, 2007). Overall, these studies indicate that the GluN2A-containing NMDARs move at the synapses thanks to mobilization of preassembled NMDARs from non-synaptic pools. However, the molecular mechanisms responsible for a selective accumulation of receptors containing the GluN2A subunit are far to be understood. We show that

Rph3A represents a needed protein in these processes thanks to its selective binding to GluN2A but not to other GluN2-type regulatory NMDAR subunits (Stanic et al., 2015). Different experimental protocols can be used to induce cLTP in dissociated hippocampal neurons, the treatment with glycine being the more commonly used (Lu et al., 2001). Here we show that induction of cLTP by using the Forskolin/Rolipram/Picrotoxin cocktail in primary cultures acts by augmenting AMPAR surface insertion and phosphorylation at GluA1-Ser845 (Joiner et al., 2010) as well as NMDAR activity/synaptic stabilization. Notably, Rph3A interaction with GluN2A plays a key role in the increase of NMDAR activity at synapses. In addition, our results show now that induction of LTP promotes accumulation of Rph3A in mushroom-type dendritic spines, where it interacts with GluN2A-containing NMDARs thus leading to synaptic retention of the receptor (Stanic et al., 2015). This event is not associated with *de novo* Rph3A protein synthesis as indicated by cLTP experiments performed in the presence of anisomycin or by the puromycin-PLA assay. Moreover, activation of the mGluR/PLC pathway plays a fundamental role in these events also confirming that Ca^{2+}/IP3 strictly modulate the capability of Rph3A to interact with protein partners (Coudevylle et al., 2008; Guillén et al., 2013).

A number of previous studies demonstrated an involvement of mGluRs/PLC pathway in both LTP and LTD. Even if the role of mGluR-dependent synaptic LTD in physiology and disease is well established (see for review Lüscher and Huber, 2010), activation of group I mGluRs through DHPG can facilitate also LTP through a PLC signaling cascade (Cohen et al., 1998; van Dam et al., 2004; Mellentin et al., 2007). Interestingly, inhibition of phospholipase C by U73122 abolished the priming of LTP induced by DHPG (Cohen et al., 1998). Moreover, the LTP induction protocol can increase the amount of GluN2A at CA1 synapses in a mGluR5 and NMDAR-dependent manner (Matta et al., 2011). In particular, in hippocampal CA1 pyramidal neurons, the developmental GluN2A/GluN2B switch driven acutely by activity requires activation of NMDARs and mGluR5 and it involves PLC activation (Matta et al., 2011). Here, we demonstrate that *in vitro* activation of PLC is essential for cLTP-associated biochemical and morphological plasticity, driving Rph3A/GluN2A summon in PSD. Furthermore, activation of different PLC-grouped metabotropic receptors increased Rph3A protein levels at synapses, indicating PLC as a key enzyme upstream of Rph3A/GluN2A complex formation.

Furthermore, Rph3A silencing or disruption of Rph3A/NMDAR complex by an interfering peptide not only blocks GluN2A accumulation at postsynaptic membranes but also prevents the induction of LTP and formation of new spines. Notably, treatment of animals with either Rph3A silencing or cell permeable peptide disrupting Rph3A/NMDAR complex impairs the acquisition of spatial memories.

Our data are in close agreement with previous reports showing that rising of hippocampal GluN1/GluN2A NMDARs at synapses appears to be a general feature after novel spatial memory acquisition (Cercato et al., 2017). As reviewed by Baez et al. (2018), the GluN1/GluN2A subunits increase at synapse starting from about 20 to 30 min after plasticity induction or memory acquisition could represent a check point or a synaptic tag for plasticity establishment or memory consolidation (Baez et al., 2018). Overall, our results demonstrate that GluN2A interaction with Rph3A is needed for NMDAR stabilization in hippocampal PSD after LTP induction and to trigger downstream signaling necessary for LTP synaptic adaptation and cognitive behavior.

Limitations of the Study

Even if our results strengthen the putative role of Rph3A as an attractive pharmacological target for several neurological conditions in which GluN2A-containing NMDARs are not correctly functioning (Sanz-Clemente et al., 2013; Lai et al., 2014; Shohami and Biegon, 2014; Gardoni and Bellone, 2015; Mellone et al., 2015), additional long-term studies in disease models are needed to confirm the involvement of Rph3A and Rph3A/GluN2A complex in these brain disorders.

METHODS

All methods can be found in the accompanying Transparent Methods supplemental file.

SUPPLEMENTAL INFORMATION

Supplemental Information can be found online at https://doi.org/10.1016/j.isci.2019.08.036.

ACKNOWLEDGMENTS

This work was supported by a PRIN 2015 grant of the Ministero dell'Istruzione, dell'Universita' e della Ricerca to F.G. (2015FNWP34) and by a Ricerca Finalizzata Grant 2013 of the Ministero della Salute to F.G..

AUTHOR CONTRIBUTIONS

Investigation, L.F., J.S., E.Z., M.M., N.C., C.R., S.M., C.B., L.P., M.S., and G.O.; Formal analysis, L.F., J.S., E.Z., M.M., N.C., C.R., S.M., C.B., L.P., and M.S.; Methodology, A.P., M.S., and L.F.; Conceptualization, F.G., M.D.L., and E.M.; Writing – Original Draft, L.C., J.S., and F.G.; Writing – Review & Editing F.G., E.M., M.D.L., C.M., N.C., and C.R.; Supervision, F.G. and M.D.L.; Project administration and Funding Acquisition, F.G.

DECLARATION OF INTERESTS

The authors declare that they have no competing interests.

Received: April 25, 2019
Revised: June 24, 2019
Accepted: August 21, 2019
Published: September 27, 2019

REFERENCES

Baez, M.V., Oberholzer, M.V., Cercato, M.C., Snitcofsky, M., Aguirre, A.I., and Jerusalinsky, D.A. (2013). NMDA receptor subunits in the adult rat hippocampus undergo similar changes after 5 minutes in an open field and after LTP induction. PLoS One *8*, e55244.

Baez, M.V., Cercato, M.C., and Jerusalinsky, D.A. (2018). NMDA receptor subunits change after synaptic plasticity induction and learning and memory acquisition. Neural Plast. *2018*, 5093048.

Barria, A., and Malinow, R. (2002). Subunit-specific NMDA receptor trafficking to synapses. Neuron *35*, 345–353.

Bellone, C., and Nicoll, R.A. (2007). Rapid bidirectional switching of synaptic NMDA receptors. Neuron *55*, 779–785.

Bonfiglio, T., Vergassola, M., Olivero, G., and Pittaluga, A. (2018). Environmental training and synaptic functions in young and old brain: a presynaptic perspective. Curr. Med. Chem., [Epub ahead of print].

Burns, M.E., Sasaki, T., Takai, Y., and Augustine, G.J. (1998). Rabphilin-3A: a multifunctional regulator of synaptic vesicle traffic. J. Gen. Physiol. *111*, 243–255.

Cercato, M.C., Vázquez, C.A., Kornisiuk, E., Aguirre, A.I., Colettis, N., Snitcofsky, M., Jerusalinsky, D.A., and Baez, M.V. (2017). GluN1 and GluN2A NMDA receptor subunits increase in the hippocampus during memory consolidation in the rat. Front. Behav. Neurosci. *10*, 242.

Chidambaram, S.B., Rathipriya, A.G., Bolla, S.R., Bhat, A., Ray, B., Mahalakshmi, A.M., Manivasagam, T., Thenmozhi, A.J., Essa, M.M., Guillemin, G.J., et al. (2019). Dendritic spines: Revisiting the physiological role. Prog. Neuropsychopharmacol. Biol. Psychiatry *92*, 161–193.

Chuang, S.C., Bianchi, R., Kim, D., Shin, H.S., and Wong, R.K. (2001). Group I metabotropic glutamate receptors elicit epileptiform discharges in the hippocampus through PLCbeta1 signaling. J. Neurosci. *21*, 6287–6294.

Cohen, A.S., Raymond, C.R., and Abraham, W.C. (1998). Priming of long-term potentiation induced by activation of metabotropic glutamate receptors coupled to phospholipase C. Hippocampus *8*, 160–170.

Coudevylle, N., Montaville, P., Leonov, A., Zweckstetter, M., and Becker, S. (2008). Structural determinants for Ca2+ and phosphatidylinositol 4,5-bisphosphate binding by the C2A domain of rabphilin-3A. J. Biol. Chem. *283*, 35918–35928.

Dieck, S., Kochen, L., Hanus, C., Heumüller, M., Bartnik, I., Nassim-Assir, B., Merk, K., Mosler, T., Garg, S., Bunse, S., et al. (2015). Direct visualization of newly synthesized target proteins in situ. Nat. Methods *12*, 411–414.

Dinamarca, M.C., Guzzetti, F., Karpova, A., Lim, D., Mitro, N., Musardo, S., Mellone, M., Marcello, E., Stanic, J., Samaddar, T., et al. (2016). Ring finger protein 10 is a novel synaptonuclear messenger encoding activation of NMDA receptors in hippocampus. Elife *5*, e12430.

Esteban, J.A., Shi, S.H., Wilson, C., Nuriya, M., Huganir, R.L., and Malinow, R. (2003). PKA phosphorylation of AMPA receptor subunits controls synaptic trafficking underlying plasticity. Nat. Neurosci. *6*, 136–143.

Ferrer-Orta, C., Pérez-Sánchez, M.D., Coronado-Parra, T., Silva, C., López-Martínez, D., Baltanás-Copado, J., Gómez-Fernández, J.C., Corbalán-García, S., and Verdaguer, N. (2017). Structural characterization of the Rabphilin-3A-SNAP25 interaction. Proc. Natl. Acad. Sci. U S A *114*, E5343–E5351.

Foster, K.A., McLaughlin, N., Edbauer, D., Phillips, M., Bolton, A., Constantine-Paton, M., and Sheng, M. (2010). Distinct roles of NR2A and NR2B cytoplasmic tails in long-term potentiation. J. Neurosci. *30*, 2676–2685.

Gallagher, S.M., Daly, C.A., Bear, M.F., and Huber, K.M. (2004). Extracellular signal-regulated protein kinase activation is required for metabotropic glutamate receptor-dependent long-term depression in hippocampal area CA1. J. Neurosci. *24*, 4859–4864.

Gardoni, F., Picconi, B., Ghiglieri, V., Polli, F., Bagetta, V., Bernardi, G., Cattabeni, F., Di Luca, M., and Calabresi, P. (2006). A critical interaction between NR2B and MAGUK in L-DOPA induced dyskinesia. J. Neurosci. *26*, 2914–2922.

Gardoni, F., and Bellone, C. (2015). Modulation of the glutamatergic transmission by Dopamine: a focus on Parkinson, Huntington and Addiction diseases. Front. Cell. Neurosci. *9*, 25.

Gottschalk, W.A., Jiang, H., Tartaglia, N., Feng, L., Figurov, A., and Lu, B. (1999). Signaling mechanisms mediating BDNF modulation of synaptic plasticity in the hippocampus. Learn. Mem. *6*, 243–256.

Grilli, M., Zappettini, S., Zanardi, A., Lagomarsino, F., Pittaluga, A., Zoli, M., and Marchi, M. (2009). Exposure to an enriched environment selectively increases the functional response of the presynaptic NMDA receptors which modulate noradrenaline release in mouse hippocampus. J. Neurochem. *110*, 1598–1606.

Grosshans, D.R., Clayton, D.A., Coultrap, S.J., and Browning, M.D. (2002). LTP leads to rapid surface expression of NMDA but not AMPA receptors in adult rat CA1. Nat. Neurosci. *5*, 27–33.

Guillén, J., Ferrer-Orta, C., Buxaderas, M., Pérez-Sánchez, D., Guerrero-Valero, M., Luengo-Gil, G., Pous, J., Guerra, P., Gómez-Fernández, J.C., Verdaguer, N., et al. (2013). Structural insights into the Ca2+ and PI(4,5)P2 binding modes of the C2 domains of rabphilin 3A and synaptotagmin 1. Proc. Natl. Acad. Sci. U S A *110*, 20503–20508.

Hannan, A.J., Blakemore, C., Katsnelson, A., Vitalis, T., Huber, K.M., Bear, M., Roder, J., Kim,

D., Shin, H.S., and Kind, P.C. (2001). PLC-beta1, activated via mGluRs, mediates activity-dependent differentiation in cerebral cortex. Nat. Neurosci. *4*, 282–288.

Horak, M., Petralia, R.S., Kaniakova, M., and Sans, N. (2014). ER to synapse trafficking of NMDA receptors. Front. Cell. Neurosci. *8*, 394.

Hu, H., Real, E., Takamiya, K., Kang, M.G., Ledoux, J., Huganir, R.L., and Malinow, R. (2007). Emotion enhances learning via norepinephrine regulation of AMPA-receptor trafficking. Cell *131*, 160–173.

Joiner, M.L., Lisé, M.F., Yuen, E.Y., Kam, A.Y., Zhang, M., Hall, D.D., Malik, Z.A., Qian, H., Chen, Y., Ulrich, J.D., et al. (2010). Assembly of a beta2-adrenergic receptor–GluR1 signalling complex for localized cAMP signalling. EMBO J. *29*, 482–495.

Kellermayer, B., Ferreira, J.S., Dupuis, J., Levet, F., Grillo-Bosch, D., Bard, L., Linarès-Loyez, J., Bouchet, D., Choquet, D., Rusakov, D.A., et al. (2018). Differential nanoscale topography and functional role of GluN2-NMDA receptor subtypes at glutamatergic synapses. Neuron *100*, 106–119.e7.

Kannangara, T.S., Eadie, B.D., Bostrom, C.A., Morch, K., Brocardo, P.S., and Christie, B.R. (2015). GluN2A-/- mice lack bidirectional synaptic plasticity in the dentate gyrus and perform poorly on spatial pattern separation tasks. Cereb. Cortex *25*, 2102–2113.

Kiyama, Y., Manabe, T., Sakimura, K., Kawakami, F., Mori, H., and Mishina, M. (1998). Increased thresholds for long-term potentiation and contextual learning in mice lacking the NMDA-type glutamate receptor epsilon1 subunit. J. Neurosci. *18*, 6704–6712.

Kullmann, D.M., and Lamsa, K.P. (2007). Long-term synaptic plasticity in hippocampal interneurons. Nat. Rev. Neurosci. *8*, 687–699.

Lai, T.W., Zhang, S., and Wang, Y.T. (2014). Excitotoxicity and stroke: identifying novel targets for neuroprotection. Prog. Neurobiol. *115*, 157–188.

Li, C., Takei, K., Geppert, M., Daniell, L., Stenius, K., Chapman, E.R., Jahn, R., De Camilli, P., and Südhof, T.C. (1994). Synaptic targeting of rabphilin-3A, a synaptic vesicle Ca2+/phospholipid-binding protein, depends on rab3A/3C. Neuron *13*, 885–898.

Liu, L., Wong, T.P., Pozza, M.F., Lingenhoehl, K., Wang, Y., Sheng, M., Auberson, Y.P., and Wang, Y.T. (2004). Role of NMDA receptor subtypes in governing the direction of hippocampal synaptic plasticity. Science *304*, 1021–1024.

Lu, W., Man, H., Ju, W., Trimble, W.S., MacDonald, J.F., and Wang, Y.T. (2001). Activation of synaptic NMDA receptors induces membrane insertion of new AMPA receptors and LTP in cultured hippocampal neurons. Neuron *29*, 243–254.

Lüscher, C., and Huber, K.M. (2010). Group 1 mGluR-dependent synaptic long-term depression: mechanisms and implications for circuitry and disease. Neuron *65*, 445–459.

Lussier, M.P., Sanz-Clemente, A., and Roche, K.W. (2015). Dynamic regulation of N-Methyl-d-aspartate (NMDA) and α-Amino-3-hydroxy-5-methyl-4-isoxazolepropionic acid (AMPA) receptors by posttranslational modifications. J. Biol. Chem. *290*, 28596–28603.

Lynch, M.A. (2004). Long-term potentiation and memory. Physiol. Rev. *84*, 87–136.

Makino, Y., Johnson, R.C., Yu, Y., Takamiya, K., and Huganir, R.L. (2011). Enhanced synaptic plasticity in mice with phosphomimetic mutation of the GluA1 AMPA receptor. Proc. Natl. Acad. Sci. U S A *108*, 8450–8455.

Malinverno, M., Carta, M., Epis, R., Marcello, E., Verpelli, C., Cattabeni, F., Sala, C., Mulle, C., Di Luca, M., and Gardoni, F. (2010). Synaptic localization and activity of ADAM10 regulate excitatory synapses through N-cadherin cleavage. J. Neurosci. *30*, 16343–16355.

Marcello, E., Saraceno, C., Musardo, S., Vara, H., de la Fuente, A.G., Pelucchi, S., Di Marino, D., Borroni, B., Tramontano, A., Pérez-Otaño, I., et al. (2013). Endocytosis of synaptic ADAM10 in neuronal plasticity and Alzheimer's disease. J. Clin. Invest. *123*, 2523–2538.

Matta, J.A., Ashby, M.C., Sanz-Clemente, A., Roche, K.W., and Isaac, J.T. (2011). mGluR5 and NMDA receptors drive the experience- and activity-dependent NMDA receptor NR2B to NR2A subunit switch. Neuron *70*, 339–351.

Mellentin, C., Jahnsen, H., and Abraham, W.C. (2007). Priming of long-term potentiation mediated by ryanodine receptor activation in rat hippocampal slices. Neuropharmacology *52*, 118–125.

Mellone, M., Stanic, J., Hernandez, L.F., Iglesias, E., Zianni, E., Longhi, A., Prigent, A., Picconi, B., Calabresi, P., Hirsch, E.C., et al. (2015). NMDA receptor GluN2A/GluN2B subunit ratio as synaptic trait of levodopa-induced dyskinesias: from experimental models to patients. Front. Cell. Neurosci. *9*, 245.

Montaville, P., Coudevylle, N., Radhakrishnan, A., Leonov, A., Zweckstetter, M., and Becker, S. (2008). The PIP2 binding mode of the C2 domains of rabphilin-3A. Protein Sci. *17*, 1025–1034.

Morris, R.G., Anderson, E., Lynch, G.S., and Baudry, M. (1986). Selective impairment of learning and blockade of long-term potentiation by an N-methyl-D-aspartate receptor antagonist, AP5. Nature *319*, 774–776.

Nakazawa, T., Komai, S., Tezuka, T., Hisatsune, C., Umemori, H., Semba, K., Mishina, M., Manabe, T., and Yamamoto, T. (2001). Characterization of Fyn-mediated tyrosine phosphorylation sites on GluR epsilon 2 (NR2B) subunit of the N-methyl-D-aspartate receptor. J. Biol. Chem. *276*, 693–699.

Oh, M.C., Derkach, V.A., Guire, E.S., and Soderling, T.R. (2006). Extrasynaptic membrane trafficking regulated by GluR1 serine 845 phosphorylation primes AMPA receptors for long-term potentiation. J. Biol. Chem. *281*, 752–758.

Otmakhov, N., Khibnik, L., Otmakhova, N., Carpenter, S., Riahi, S., Asrican, B., and Lisman, J. (2004). Forskolin-induced LTP in the CA1 hippocampal region is NMDA receptor dependent. J. Neurophysiol. *91*, 1955–1962.

Paoletti, P., Bellone, C., and Zhou, Q. (2013). NMDA receptor subunit diversity: impact on receptor properties, synaptic plasticity and disease. Nat. Rev. Neurosci. *14*, 383–400.

Papouin, T., Ladépêche, L., Ruel, J., Sacchi, S., Labasque, M., Hanini, M., Groc, L., Pollegioni, L., Mothet, J.P., and Oliet, S.H. (2012). Synaptic and extrasynaptic NMDA receptors are gated by different endogenous coagonists. Cell *150*, 633–646.

Peng, Y., Zhao, J., Gu, Q.H., Chen, R.Q., Xu, Z., Yan, J.Z., Wang, S.H., Liu, S.Y., Chen, Z., and Lu, W. (2010). Distinct trafficking and expression mechanisms underlie LTP and LTD of NMDA receptor-mediated synaptic responses. Hippocampus *20*, 646–658.

Philpot, B.D., Sekhar, A.K., Shouval, H.Z., and Bear, M.F. (2001). Visual experience and deprivation bidirectionally modify the composition and function of NMDA receptors in visual cortex. Neuron *29*, 157–169.

Philpot, B.D., Espinosa, J.S., and Bear, M.F. (2003). Evidence for altered NMDA receptor function as a basis for metaplasticity in visual cortex. J. Neurosci. *23*, 5583–5588.

Philpot, B.D., Cho, K.K., and Bear, M.F. (2007). Obligatory role of NR2A for metaplasticity in visual cortex. Neuron *53*, 495–502.

Sakimura, K., Kutsuwada, T., Ito, I., Manabe, T., Takayama, C., Kushiya, E., Yagi, T., Aizawa, S., Inoue, Y., Sugiyama, H., et al. (1995). Reduced hippocampal LTP and spatial learning in mice lacking NMDA receptor epsilon 1 subunit. Nature *373*, 151–155.

Sanz-Clemente, A., Nicoll, R.A., and Roche, K.W. (2013). Diversity in NMDA receptor composition: many regulators, many consequences. Neuroscientist *19*, 62–75.

Sawtell, N.B., Frenkel, M.Y., Philpot, B.D., Nakazawa, K., Tonegawa, S., and Bear, M.F. (2003). NMDA receptor-dependent ocular dominance plasticity in adult visual cortex. Neuron *38*, 977–985.

Shipton, O.A., and Paulsen, O. (2013). GluN2A and GluN2B subunit-containing NMDA receptors in hippocampal plasticity. Philos. Trans. R. Soc. Lond. B Biol. Sci. *369*, 20130163.

Shohami, E., and Biegon, A. (2014). Novel approach to the role of NMDA receptors in traumatic brain injury. CNS Neurol. Disord. Drug Targets *13*, 567–573.

Sprengel, R., Suchanek, B., Amico, C., Brusa, R., Burnashev, N., Rozov, A., Hvalby, O., Jensen, V., Paulsen, O., Andersen, P., et al. (1998). Importance of the intracellular domain of NR2 subunits for NMDA receptor function in vivo. Cell *92*, 279–289.

Stanic, J., Carta, M., Eberini, I., Pelucchi, S., Marcello, E., Genazzani, A.A., Racca, C., Mulle, C., Di Luca, M., and Gardoni, F. (2015). Rabphilin 3A retains NMDA receptors at synaptic sites through interaction with GluN2A/PSD-95 complex. Nat. Commun. *6*, 10181.

Stanic, J., Mellone, M., Napolitano, F., Racca, C., Zianni, E., Minocci, D., Ghiglieri, V., Thiolat, M.L., Li, Q., Longhi, A., et al. (2017). Rabphilin 3A: a novel target for the treatment of levodopa-induced dyskinesias. Neurobiol. Dis. *108*, 54–64.

Summa, M., Di Prisco, S., Grilli, M., Marchi, M., and Pittaluga, A. (2011). Hippocampal AMPA autoreceptors positively coupled to NMDA autoreceptors traffic in a constitutive manner and undergo adaptative changes following enriched environment training. Neuropharmacology *61*, 1282–1290.

Swanger, S.A., and Traynelis, S.F. (2018). Synaptic receptor diversity revealed across space and time. Trends Neurosci. *41*, 486–488.

van Dam, E.J., Kamal, A., Artola, A., de Graan, P.N., Gispen, W.H., and Ramakers, G.M. (2004). Group I metabotropic glutamate receptors regulate the frequency-response function of hippocampal CA1 synapses for the induction of LTP and LTD. Eur. J. Neurosci. *19*, 112–118.

Yang, M., and Leonard, J.P. (2001). Identification of mouse NMDA receptor subunit NR2A C-terminal tyrosine sites phosphorylated by coexpression with v-Src. J. Neurochem. *277*, 580–588.

Yashiro, K., Corlew, R., and Philpot, B.D. (2005). Visual deprivation modifies both presynaptic glutamate release and the composition of perisynaptic/extrasynaptic NMDA receptors in adult visual cortex. J. Neurosci. *25*, 11684–11692.

ISCI, Volume *19*

Supplemental Information

Linking NMDA Receptor Synaptic Retention to Synaptic Plasticity and Cognition

Luca Franchini, Jennifer Stanic, Luisa Ponzoni, Manuela Mellone, Nicolò Carrano, Stefano Musardo, Elisa Zianni, Guendalina Olivero, Elena Marcello, Anna Pittaluga, Mariaelvina Sala, Camilla Bellone, Claudia Racca, Monica Di Luca, and Fabrizio Gardoni

Supplementary Figures

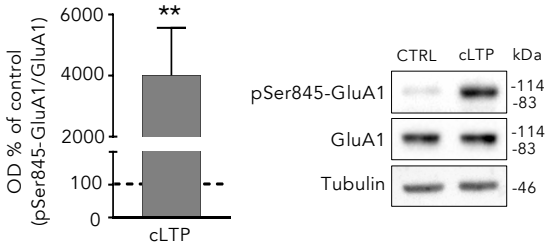

Figure S1 - GluA1 Ser845 phosphorylation levels after induction of cLTP, related to Figure 2.

Bar graph and representative blots of GluA1 and phosphorylation of GluA1 at Ser845 in TIF from primary cultures undergone cLTP. **p<0.01, t test, n=9. Molecular weight markers are indicated on the right.

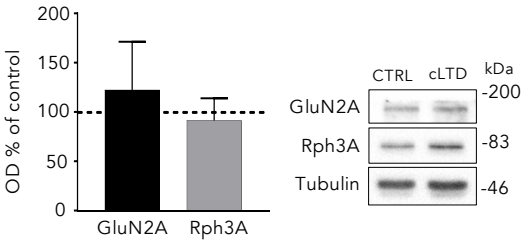

Figure S2 - GluN2A and Rph3A synaptic localization after induction of cLTD, related to Figure 2.

Application of cLTD did not affect protein levels for Rph3A and GluN2A in TIF as displayed through immunoblot. Molecular weight markers are indicated on the right.

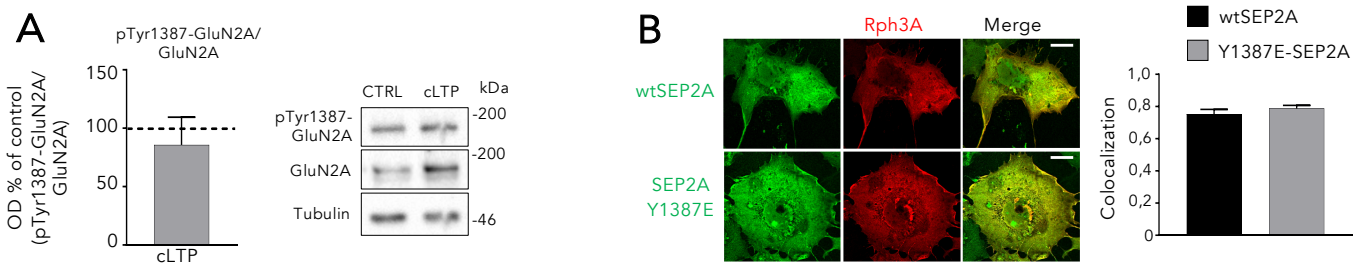

Figure S3 - GluN2A phosphorylation in Tyr1387 does not regulate GluN2A/Rph3A complex formation following LTP induction, related to Figure 3.

(A) Western blot analysis of GluN2A Tyr1387 phosphorylation normalized on GluN2A total levels in TIF of hippocampal primary cultures after cLTP (t-test, n=3). Molecular weight markers are indicated on the right. (B) Colocalization analysis between RFP-Rph3A and SEP-GluN2Awt or with single point mutation at Tyr1387 mimicking phosphorylation (Y1387E). n=13, t-test. Scale bar, 10µm.

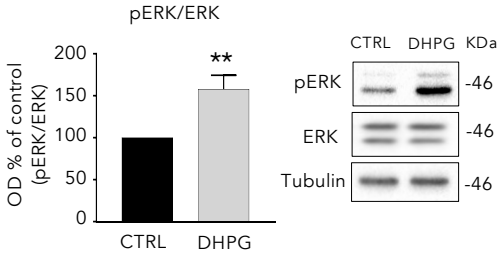

Figure S4 - Analysis of pERK phosphorylation as positive control of DHPG treatment, related to Figure 3.

Bar chart and representative blots of pERK, ERK, and tubulin performed in the homogenate from primary hippocampal cultures treated with DHPG. **p<0.01, t-test, n=10. Molecular weight markers are indicated on the right.

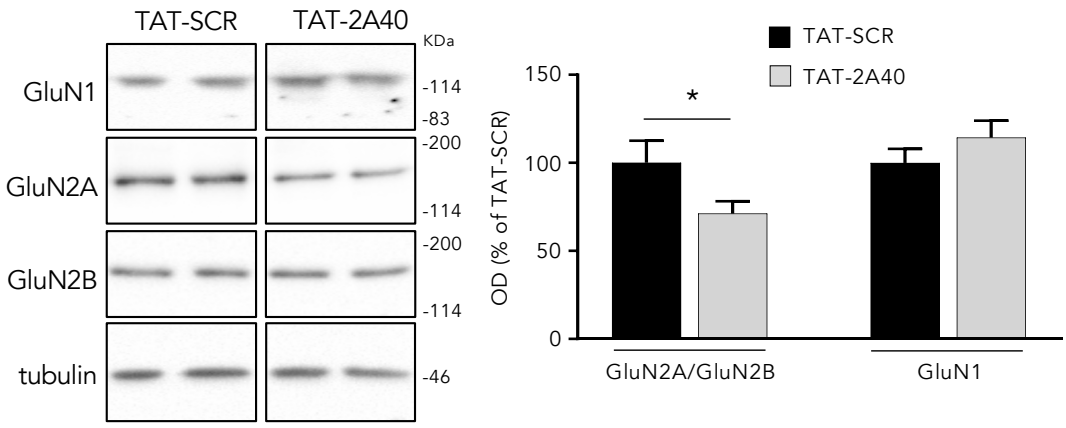

Figure S5 – Effect of *in vivo* treatment with TAT-2A40 on GluN1 and GluN2A/GluN2B ratio at synapses, related to Figure 5.

Western blot analysis of GluN1, GluN2A, GluN2B and tubulin performed in triton-insoluble postsynaptic fractions (TIF) purified from the hippocampus of rats treated with TAT-2A40 or TAT-SCR peptides (1h, 3 nmol/gr). The bar graph represents the percentage of tubulin normalized optical density of GluN2A/GluN2B and GluN1 bands of TAT-2A40 samples compared with TAT-SCR controls. *$p<0.05$, t-test, n=5. Molecular weight markers are indicated on the right.

TRANSPARENT METHODS

Enriched Environment (EE) - Mice (5 weeks old female, strain C57BL/6J) were obtained from Charles River (Calco, Italy) and were housed in the animal facility of the Department of Pharmacy, Section of Pharmacology and Toxicology, School of Medical and Pharmaceutical Sciences, University of Genoa (authorization n. 484 of 2004). After three days, mice were housed for three months in standard or in enriched conditions (see below) and then they were sacrificed by cervical dislocation and immediately decapitated to collect cerebral tissues. The experimental procedures were in accordance with the European legislation (Directive 2010/63/EU for animal experiments), the ARRIVE guidelines and the 8th Edition of the "Guide for the care and Use in laboratory-animals", and they were approved by the Animal Subjects Review Board of the University of Genoa and by the Italian Ministry of Health (DDL 26/2014 and previous legislation; protocol n. 50/2011-B and 612/2015-PR).

Female mice were randomly assigned to two different groups: the untrained mice and the enriched environmental trained mice. Trained animals were housed in a large cage (36 x 54 x 19 cm, 8 animals *per* cage) containing a variety of objects such as plastic tunnels, climbing ladders, running wheels, toys in wood and plastic suspended from the ceiling, paper, cardboard boxes, and nesting material. Objects were changed every 3 days. Untrained animals were housed in a standard cage with nest. In both cases, the bedding was changed every week. The animals were kept in the enriched environment for three months.

Spatial object recognition - Mice (6 weeks old male, strain C57BL/6J) were obtained from Charles River (Calco, Italy) and were housed in the animal facility of the CNR Institute of Neuroscience, Milano. Spatial object recognition test was performed one week after housing. Object location tests were performed in an arena according to the methods described in (Kenney *et al.*, 2011), with slight modifications. Two visual cues were placed on two adjacent walls of an opaque white Plexiglas cage (58 × 50 × 43 cm) that was dimly lit from above (27 lux). The visual cues consisted of a black and white striped pattern (21 × 29 cm) that was affixed to the center of the northern wall and a black and white checkered pattern (21 × 29 cm) that was placed in the center of the western wall. The objects were counterbalanced across locations. The cage and the objects were thoroughly wiped down with acetic acid (0.1%) before and after all behavioural procedures, which were observed and recorded using a camera mounted above the cage. Climbing or sitting on objects was not scored as object exploration. Twenty-four hours after 10 min habituation to the cage without objects, mice were exposed to the cage where two different objects were placed in the NE and NW corners for a maximum of 20 min or until they had completed 30 s of cumulative objects exploration and the time spent exploring the objects was recorded. Two hours later, the object the mouse had spent more time

exploring in the previous session (T1 phase) was moved to the SW corner of the cage, and each mouse was allowed to re-explore the cage (T2 phase). Exploration was defined as a mouse having its nose directed toward the object and within approximately 1 cm of the object. TAT-SCR or TAT-2A40 treatment was done 60 min before T1 phase. Performance was evaluated by calculating a discrimination index (N-F/N+F), where N = the time spent exploring the moved object during T2, and F = the time spent exploring the stationary object during T2.

Spontaneous motor activity - Motor function was evaluated in an automated activity cage (43 x 43 x 32 cm; Ugo Basile) placed in a sound-attenuating room. The cage was fitted with two parallel horizontal and vertical infrared beams located 2 and 4 cm from the floor, respectively. Before the start of the test, each mouse was habituated to the testing room for 1 h. Cumulative horizontal and vertical movement counts were recorded for 10 min. The test was carried out in the same animals submitted to Spatial Object Recognition test, immediately after T2 phase of Spatial Object Recognition test (Sala *et al.*, 2011).

Cell Cultures - Primary neuronal cultures were prepared from embryonic day 18-19 (E18-E19) rat hippocampi (Piccoli *et al.*, 2007). Neurons were transfected at *DIV9* through Calcium-Phosphate co-precipitation method with 2-4μg of DNA for GFP (plasmid kindly provided by Dr. Maria Passafaro), tGFP-shRph3A or tGFP-shScramble. Procedures on rats were carried out according to the European Communities Council Directive 2010/63/EU and the current Italian Law on the welfare of the laboratory animal (D.Lgs. n. 26/2014). Procedures were approved by the Italian Ministry of Health (authorizazion n. 326/2015).

COS7 cells were grown on 100 mm dishes and maintained in DMEM containing Glutamax (DMEM+Glutamax, GIBCO) supplemented with 10% fetal bovine serum and penicillin–streptomycin (GIBCO). Cells were allowed to grow till confluence before passaging every 3–4 days using trypsin. COS-7 cells were placed in a 12 wells multiwell and transfected with 250–500 ng of plasmid DNA (RFP-Rph3A; eGFP-GluN2A; eGFP-GluN2A(Y1387E) the lipofectamine LTX method (Invitrogen). After 36 h, COS-7 cells were fixed for immunostaining.

Pre-embedding immunohistochemistry - Three Sprague Dawley adult male rats were used. After terminal anesthesia was induced by brief inhalation of isoflurane (0.05% in air), followed by an intramuscular injection of ketamine (100 mg kg^{-1}) and xylazine (10 mg kg^{-1}), rats were intracardially perfused with 4% paraformaldehyde (PFA) and 0.1% glutaraldehyde in phosphate buffer saline (PBS, 0.1 M, pH 7.2), and brain sections (100 μm) were cut on a Leica VT1000S vibratome (Leica Microsystems, Milton Keynes, UK). All procedures were performed according to the requirements of the United Kingdom Animals (Scientific Procedures) Act 1986, Newcastle University AWERB 596. The vibratome sections were collected in PBS and then incubated in 50 mM ammonium chloride

in PBS for 20 min at RT. After extensive washing in PBS, antigen retrieval was performed by incubation of the sections in 10 mM sodium citrate, pH 8.4, for 1 h at 80°C. Sections were once more extensively washed with PBS before being blocked in 0.1% (w/v) gelatin in PBS. Sections were incubated with rabbit anti-Rph3A polyclonal antibody (1:100; ab68857, Abcam) in 0.1% (w/v) gelatin, 0.05% Triton X-100 in PBS at 4°C for 48–72 h. Sections were rinsed in PBS, postfixed for 5 min in 4% PFA in PBS, rinsed again, and incubated with biotin-conjugated goat anti-rabbit secondary antibody (1:200) for 12 h in 0.8% bovine serum albumin and 0.2% fish gelatin (Sigma-Aldrich) in PBS at 4°C. The following day, sections were rinsed in PBS, then postfixed in 1% glutaraldehyde in PBS (5 min) and rinsed in PBS followed by ABC Elite Kit (1:200; 2 h at RT) (Vector Laboratories). The peroxidase reaction was revealed by incubating the sections in ImmPACT VIP substrate Kit (Vector Laboratories). Then the sections were osmicated, dehydrated, and flat embedded in Durcupan resin (Sigma-Aldrich). Ultrathin sections (70–90 nm) were countercolored with uranyl acetate and lead citrate. Control experiments, in which the primary antibody was omitted, resulted in no immunoreactivity. The images were captured with an AMT XR404 megapixel side mounted CDD camera at a magnification between 7900 and 92000. Only identified synapses on dendritic spines of apical dendrites of pyramidal cells in *stratum radiatum* of CA1 hippocampus were included in the analysis. No tangentially cut synapses were analysed. To determine the spine density (number of spines/μm^2), we utilized 28-35 images per animal (7900 magnification, Tot Area: 7841.306μm^2) in which we identified the spines and, then, quantified them using the cell counter tool in ImageJ (http://rsb.info.nih.gov/ij). Morphometric parameters such as spine head area, PSD length, and thickness (Moreau *et al.*, 2010) were measured from 500 spines/animal. To determine the head area of spines, we traced the plasma membrane with ImageJ. The average thickness of the PSDs was measured as follow: the cytoplasmic outline of a PSD, including the associated dense material, was traced with ImageJ, and this area was then enclosed by tracing the postsynaptic membrane (length of PSD). The area was then divided by the length of the postsynaptic membrane to derive an average thickness for the PSD. The results are presented as the mean ± SEM. The measurements were all performed by experimenters blind to the genotype.

Cell fractionation and postsynaptic density purification – Crude membrane (P2) and Triton-insoluble (TIF) fractions were isolated from rat hippocampal primary cultures and mice hippocampi. TIF is highly enriched in postsynaptic densities proteins (Gardoni *et al.*, 2006). Samples were homogenized at 4°C in an ice-cold buffer containing 0.32 M Sucrose, 0.1 mM phenylmethylulfonyl fluoride (PMSF), 1 mM Hepes, 1 mM MgCl, 1 mM NaF supplemented with protease inhibitor (Complete™, Sigma-Aldrich) and phosphatase inhibitors (PhosSTOP™, Sigma-Aldrich). The homogenate was centrifuged at 1,000g for 5 minutes at 4°C to remove nuclear fractions and white

matter. The supernatant was centrifuged at 13,000g for 15 min at 4°C; the resulting pellet representing P2 fraction, was resuspended in 1% Triton-X-100 and 75 mM KCl for 15 minutes at 4°C. Samples were centrifuged at 100,000g for 1 h at 4 °C and the pellets obtained representing the TIF were resuspended in 20 mM HEPES.

Immunocytochemistry (ICC) - For colocalization and morphological studies, GFP-transfected hippocampal neurons were fixed for 5 min at 4ºC in 4% PFA plus 4% sucrose in Dulbecco's Phosphate Buffered Saline (PBS; Sigma-Aldrich). Coverslips were then washed with PBS, permeabilized with 0,1% triton X-100 in PBS for 15 min at room temperature and blocked for 30 minutes at room temperature with 5% Bovine Serum Albumin (BSA) in PBS. Cells were then incubated with primary antibodies in 5% BSA-PBS overnight at 4ºC in a humid chamber. After washes with PBS, the cells were incubated with the fluorophore-conjugated secondary antibodies in 5% BSA-PBS for 1h at room temperature in a humid chamber protected from light. The incubation was followed by washes with PBS and mounting on glass slides using Fluoroshield mounting medium (Sigma-Aldrich). For GluN2A surface/total staining assay, cells were fixed with 4% Paraformaldehyde (PFA)-4% sucrose in PBS solution at 4°C for 5 min and washed several times with PBS. Cells were then blocked with 5% BSA in PBS for 30 min at room temperature and then labelled with primary antibody for surface labelling of extracellular epitopes for 1 h at room temperature (or overnight at 4°C). Cells were washed and then incubated with secondary antibody for 1 h at room temperature. Cells were then washed with PBS and permeabilized with 0.1% Triton X-100 in PBS for 15 min at room temperature and blocked with 5% BSA in PBS for 30 min at room temperature. Cells were then labelled with antibodies for intracellular epitopes for 1 h at room temperature or overnight at 4 °C. Cells were washed and then incubated with secondary antibodies for 1 h at room temperature. Cells were then washed in PBS and mounted on glass slides with Fluoromount mounting medium (Sigma Aldrich).

Proximity ligation assay (PLA) - Primary hippocampal cultures were transfected with GFP at *DIV9*, treated at DIV15 and then fixed with 4%PFA in PBS + 4% sucrose. Coverslips were then washed 3 times with PBS and permeabilized with Triton-X-100 0,1% in PBS for 15 minutes and later blocked with 5% BSA in PBS for 30 minutes at room temperature. Coverslips were then incubated in a dark humid chamber overnight at 4°C with primary antibodies in 5% BSA in PBS, washed 3 times with PBS and then incubated with secondary antibodies conjugated with oligonucleotides (PLA probe MINUS and PLA probe PLUS) for 1 h at 37°C in a dark humid chamber. Coverslips were then washed 3 times with PBS and incubated with the ligation solution (Olink bioscience) supplemented with ligase (25 mU/µL) for 30 min at 37ºC in a dark humid chamber and washed with Wash Buffer A (NaCl 0.15 M, Tris 0.01 M, 0.05 % tween 20, pH 7.4; Olink Bioscence). The amplification solution

(containing nucleotides and fluorescently labeled oligonucleotides; Olink bioscence) supplemented with polymerase (0.125 U/μL) was added to each sample and incubated for 100 min at 37 ºC in humid dark chamber. Coverslips were then washed 3 times with decreasing concentration of Wash Buffer B (NaCl 0.1 M, Tris 0.2 M, pH 7.5; Olink bioscience).

Western Blot (WB) - Proteins were separated on a denaturing Sodium Dodecyl Sulfate - PolyAcrylamide Gel Electrophoresis (SDS-PAGE) followed by western blotting onto nitrocellulose membranes. 10-15 μg of proteins were separated on 7% or 10% SDS-PAGE (depending on the molecular weight of the protein investigated) and transferred on nitrocellulose membrane. The membranes incubated for 1 h at room temperature in blocking solution (I-block, Tris-Buffered saline (TBS) 1X, 20% Tween-20) on a shaker. The membranes were then incubated with the specific primary antibody (Anti-Tubulin; anti-GluN2A; Anti-phosphoSer845-GluA1; Anti-Rabphilin3A; Anti-GluN2B; Anti-phosphoT202/Y204-MAPK 44/42; anti-ERK 44/42) in blocking solution overnight at 4 C° and the following day, after three washes with TBS and tween 20 (TBS + Tween-20 0.1%; TBSt), they were incubated with corresponding Horseradish Peroxidase (HRP)-conjugated secondary antibody in blocking solution for 1 h at room temperature. After washing with TBSt, membranes were developed using electrochemiluminescence (ECL) reagents (Biorad). Finally, membranes were scanned using a Chemidoc (Biorad Universal Hood III) with Image Lab software (Biorad). Bands were quantified by means of computer-assisted imaging (Image Lab, Biorad). The levels of the proteins were expressed as relative optical density (OD) measurements and normalized on tubulin and then expressed as percentage of control mean.

Co-Immunoprecipitation Assay - A measure of 50 μg of proteins from rat hippocampal primary cultures and hippocampal tissue P2 fractions were incubated on a wheel overnight at 4°C in RIA buffer 1X (200 mM NaCl, 10 mM EDTA, 10 mM Na_2HPO_4, 0.5% NP-40) plus 0.1% SDS and the rabbit anti-Rabphilin3A antibody. The day after protein A/G-agarose beads were resuspended in RIA 1x, added to the samples and incubated at room temperature on a wheel for 2 h. Beads were then sedimented and the supernatant discarded, then they were washed three times with RIA 1X + SDS 0,1%, mixed with Loading Buffer (6x) and boiled for 10’ at 96°C for Western Blot procedures.

Electrophysiology - C57BL/6J male mice were intraperitoneal injected either with TAT-2A40 or TAT-SCR peptides at 3nmol/g. After 1h mice were anesthetized with isoflurane/O_2 and brains were dissected on ice. Hippocampal coronal slices (300 μm) were cutted in cold artificial cerebrospinal fluid (ACSF) containing (in mM): 119 NaCl, 2.5 KCl, 1.3 $MgCl_2$, 2.5 $CaCl_2$, 1.0 NaH_2PO_4, 26.2 $NaHCO_3$ and 11 glucose, bubbled with 95% O_2 and 5% CO_2. Slices were maintained at room temperature and allowed to recover for 1 hr before being transferred to the recording chamber. The

external solutions contained (in mM) 119 NaCI, 2.5 KCI, 2.5 $CaCl_2$, 1.3 $MgSO_4$, 1.0 NaH_2PO_4, 26.2 $NaHCO_3$, 11 glucose, and 0.1 picrotoxin (pH 7.4) at 37°C and equilibrated with 95% O_2 and 5% CO_2. Somatic whole-cell voltage-clamp recordings were made from CA1 pyramidal cells using 2–6 ΩM electrodes. The internal solution contained (in mM) 115 $CsMeSO_4$, 20 $CsCl_2$, 10 HEPES, 2.5 $MgCl_2$, 4 NaATP, 0.4 NaGTP, 10 NaCreatine, and 0.6 EGTA (pH 7.2). Cells were held at −70 mV and LTP protocol was induced by pairing the cell at 0 mV at a frequency of 2 Hz for 90 s. Synaptic responses were collected for 25 minutes with a Multiclamp 700B-amplifier (Axon Instruments, Foster City, CA), filtered at 2 kHz, digitized at 5 Hz, and analysed online using Igor Pro software Wavemetrics, Lake Oswego, OR).

Chemical Long-Term Potentation (cLTP) and Chemical Long-Term Depression (cLTD): - cLTP was induced using a previously validated protocol (Otmakhov *et al.,* 2004; Dinamarca *et al.*, 2016). Neurons were incubated in artificial cerebrospinal fluid (ACSF, 125mM NaCl, 25mM KCl, 2 mM $CaCl_2$, 33 mM Glucose and 25 mM HEPES) + 1 mM $MgCl_2$ for 30 minutes at 37°C, then cLTP induction was performed in ACSF without $MgCl_2$, plus 50 µM Forskolin (Tocris), 0.1 µM Rolipram (Tocris) and 100 µM Picrotoxin (Tocris) for 16 minutes. Control groups were kept in normal ACSF. After that, cells incubated back in ACSF with $MgCl_2$ for 15 minutes till 2 hours, depending on the type of the experiment. To induce cLTD neuronal cultures were first incubated in ACSF for 30 minutes, then stimulated for with 50µM NMDA (Sigma-Aldrich) in ACSF (Oh *et al.*, 2006; Marcello *et al.*, 2013). After 10 minutes stimulation, NMDA solution was replaced with regular ACSF, finally cultures were homogenized for TIF preparation.

Puromycin-Proximity ligation assay (Puro-PLA) – To detect local protein synthesis, we used Puro-PLA technique (Dieck *et al.*, 2015; Li and Götz, 2017). Puromycin inserts in new synthetized polypeptides blocking their elongation. Therefore, by labeling Puromycin and the N-term fragment of a target protein with specific antibodies we were able to detect as PLA signal the newly synthetized target protein. Puro-PLA was performed on *DIV14* primary hippocampal cultures treated with cLTP. Puromycin (1µM) or vehicle were added 16 minutes after cLTP induction. Cells were then fixed 5 min at 4°C in 4% PFA plus 4% sucrose in Dulbecco's Phosphate Buffered Saline (PBS; Sigma-Aldrich). Coverslips were then washed with PBS, permeabilized with 0,1% triton X-100 in PBS for 15 minutes and blocked for 30 minutes at 37°C with Duo-Link blocking solution. Primary antibodies for Puromycin (Mouse monoclonal #MABE343; 1:100) and for Rph3A (rabbit polyclonal N-term epitope, #133961AP; 1:200) were diluted in Duo-Link Antibody Diluent and incubated with coverslips at 4°C overnight in a humid chamber. Following steps are according to the PLA protocol. Negative controls for PLA specificity were performed in absence of Puromycin as well as in absence of the Puromycin primary antibody.

Confocal Imaging - Images were taken using an inverted A1R (Nikon) or LSM510 (Zeiss) confocal microscopes. For PLA assay, analysis of GluA1 and GluN2A clusters, and morphological studies z-stacks of 0.5 µm thickness were acquired. Cells were chosen randomly for quantification from four to eight different coverslips (two to three independent experiments), images were acquired using the same settings/exposure times and at least ten cells for each condition were analyzed. Co-localization analysis was performed using AIM 4.2 software (Zeiss). Analysis of dendritic spine morphology was performed with ImageJ software; for each dendritic spine length, the head and neck width were measured, which were used to classify dendritic spines into three categories (thin, stubby and mushroom; Harris *et al.*, 1992). GluA1 cluster diameters and density as well as PLA clusters area and density were measured using ImageJ.

Reagents - We used cell permeable peptides (CPPs) TAT-2A-40 and TAT-Scr highly validated for both *in vitro* and *in vivo* studies (Stanic *et al.*, 2015, 2017) and manufactured by Bachem (Bubendorf, Switzerland). Lyophilized CPPs were resuspended in sterile deionized water to a stock concentration of 1 mM and stored at −20 °C. U73122 (#1268), Forskolin (#1099/10), Rolipram (#0905), Picrotoxin (#1128) were purchased from Tocris and solubilized in DMSO (#D2650) according to manufacturer's protocols to a stock concentration of 2 mM, 25mM, 0.1mM and 100mM, respectively. 3,5-R,S-DHPG (#HB0026) was purchased from HelloBio and dissolved in sterile deionized water to a stock concentration of 10 mM according to manufacturer's datasheet. BDNF (#AB9794, Sigma Aldrich) was used at a final concentration of 50ng/ml for 3h (Blanquet and Lamour, 1997). NMDA (#M3262) puromycin (#P8833) and anisomycin (#A9789) were purchased from Sigma-Aldrich, dissolved in sterile deionized water to a stock concentration of 500µM and 4mM respectively.

Antibodies - The following unconjugated antibodies were used: mouse anti-Tubulin (WB 1:30000; #T9026, Sigma), rabbit anti-GluN2A (WB 1:1000 #M264) were purchased from Sigma-Aldrich. Rabbit anti-phosphoTyr1387-GluN2A (1:1000 #16647) was purchased from Abcam. Mouse monoclonal anti-Puromycin (WB 1:5000 #MABE343) clone 12D10, rabbit anti-N-term GluA1 (ICC 1:100 MAB2263) and rabbit monoclonal anti-phosphoSer845-GluA1 (WB 1:1000 #04-1073) were purchased from Merck Millipore. Rabbit anti-Rabphilin3A (WB 1:1000 #118003) was purchased from Synaptic System. Rabbit anti-N-term GluN2A (ICC 1:100 480031), rabbit Anti-GluN2B (WB 1:1000 #718600), were purchased from Invitrogen. Rabbit anti-phosphoT202/Y204-MAPK 44/42 (WB 1:1000 #9101) and rabbit anti-MAPK 44/42 (WB 1:1000 #9102) were purchased from Cell Signaling. Mouse monoclonal anti-PSD-95 (WB 1:1000, ICC 1:100 #K28/43) Neuromab. Rabbit anti-tGFP (ICC 1:300 #AB513) was purchased from Evrogen. Rabbit anti-Nterm-Rph3A (Puro-PLA 1:200, #133961AP) was purchased from Proteintech. Secondary antibodies for Western Blot analysis: goat anti-Mouse Horseradish (170-6516) and goat anti-rabbit (170-6515), both

Horseradish peroxidase conjugated, were purchased from Biorad and used in Iblock solution at 1:5000-1:20000 concentration. Secondary antibodies for imaging experiments: goat anti-rabbit-Alexa555 (A-21429; Life Technologies), Alexa-fluor 488 (A-11039) goat anti-chicken, goat anti-mouse-Alexa555 (A-21422), 4',6'-diamidino-2-phenylindole (DAPI, 1:50,000 in PBS, Thermo Fischer Scientific), goat anti-rabbit-Alexa-488 (A-11034), donkey anti-rabbit-Alexa-647 (A-31573).

Statistical analysis - Data were expressed as mean ± SEM and analysed with Student's t test, one-way analysis of variance (ANOVA) or two-way analysis of variance for repeated measures followed by Tukey or Bonferroni post-hoc test as appropriate. The accepted value for significance was $p<0.05$. All statistical analyses were done using the software Prism, version 7 (GraphPad, San Diego, CA, USA).

SUPPLEMENTAL REFERENCES

Dieck, S., Kochen, L., Hanus, C., Heumüller, M., Bartnik, I., Nassim-Assir, B., Merk, K., Mosler, T., Garg, S., Bunse, S., et al (2015). Direct visualization of newly synthesized target proteins in situ. Nat. Methods *12*, 411-414.

Dinamarca, M.C., Guzzetti, F., Karpova, A., Lim, D., Mitro, N., Musardo, S., Mellone, M., Marcello, E., Stanic, J., Samaddar, T., et al (2016). Ring finger protein 10 is a novel synaptonuclear messenger encoding activation of NMDA receptors in hippocampus. Elife *5*, e12430.

Gardoni, F., Picconi, B., Ghiglieri, V., Polli, F., Bagetta, V., Bernardi, G., Cattabeni, F., Di Luca, M., and Calabresi, P. (2006). A critical interaction between NR2B and MAGUK in L-DOPA induced dyskinesia. J. Neurosci. *26*, 2914-2922.

Harris, K.M., Jensen, F.E., and Tsao, B. (1992). Three-dimensional structure of dendritic spines and synapses in rat hippocampus (CA1) at postnatal day 15 and adult ages: implications for the maturation of synaptic physiology and long-term potentiation. J. Neurosci. *12*, 2685-2705.

Kenney, J.W., Adoff, M.D., Wilkinson, D.S., and Gould, T.J. (2011). The effects of acute, chronic, and withdrawal from chronic nicotine on novel and spatial object recognition in male C57BL/6J mice. Psychopharmacology (Berl) *217*, 353-365.

Li, C., and Götz, J. (2017). Somatodendritic accumulation of Tau in Alzheimer's disease is promoted by Fyn-mediated local protein translation. EMBO J. *36*, 3120-3138.

Marcello, E., Saraceno, C., Musardo, S., Vara, H., de la Fuente, A.G., Pelucchi, S., Di Marino, D., Borroni, B., Tramontano, A., Pérez-Otaño, I., et al (2013). Endocytosis of synaptic ADAM10 in neuronal plasticity and Alzheimer's disease. J. Clin. Invest. *123*, 2523-2538.

Moreau, M.M., Piguel, N., Papouin, T., Koehl, M., Durand, C.M., Rubio, M.E., Loll, F., Richard, E.M., Mazzocco, C., Racca, C., Oliet, S.H., Abrous, D.N., Montcouquiol, M., Sans, N. (2010). The planar polarity protein Scribble1 is essential for neuronal plasticity and brain function. J Neurosci. *30*, 9738-9752.

Oh, M.C., Derkach, V.A., Guire, E.S., and Soderling, T.R. (2006). Extrasynaptic membrane trafficking regulated by GluR1 serine 845 phosphorylation primes AMPA receptors for long-term potentiation. J. Biol. Chem. *281*, 752-758.

Otmakhov, N., Khibnik, L., Otmakhova, N., Carpenter, S., Riahi, S., Asrican, B., and Lisman, J. (2004). Forskolin-induced LTP in the CA1 hippocampal region is NMDA receptor dependent. J. Neurophysiol. *91*, 1955-1962.

Piccoli, G., Verpelli, C., Tonna, N., Romorini, S., Alessio, M., Nairn, A.C., Bachi, A., and Sala, C. (2007). Proteomic analysis of activity-dependent synaptic plasticity in hippocampal neurons. J Proteome Res. *6*, 3203-3215.

Sala, M., Braida, D., Lentini, D., Busnelli, M., Bulgheroni, E., Capurro, V., Finardi, A., Donzelli, A., Pattini, L., Rubino, T., et al (2011). Pharmacologic rescue of impaired cognitive flexibility, social deficits, increased aggression, and seizure susceptibility in oxytocin receptor null mice: a neurobehavioral model of autism. Biol. Psychiatry *69*, 875-882.